ZEB1 Is a Key Regulator of Cardiomyocyte Structure and Function

Parul Gupta[1,2], Daniel Finke[1,2], Verena Kamuf-Schenk[1,2], Anushka Deshpande[1,2], Marc P. Stemmler[3], Simone Brabletz[3], Thomas Brabletz[3], Norbert Frey[1,2], Tobias Jakobi[4], Mirko Völkers[1,2] and Vivien Kmietczyk[1,2]

[1] Department of Internal Medicine III (Cardiology, Angiology, and Pneumology), Heidelberg University Hospital, 69120 Heidelberg, Germany.

[2] DZHK (German Center for Cardiovascular Research), Partner Site Heidelberg/Mannheim, 69120 Heidelberg, Germany.

[3] Department of Experimental Medicine I, Friedrich-Alexander-University of Erlangen-Nuernberg, 91054 Erlangen, Germany

[4] Department of Internal Medicine and the Translational Cardiovascular Research Center, University of Arizona College of Medicine - Phoenix, Phoenix, USA.

* Correspondence to: Vivien Kmietczyk and Mirko Völkers, University Hospital Heidelberg, Department of Cardiology, Angiology, and Pneumology, Internal Medicine III, Im Neuenheimer Feld 410, 69120 Heidelberg, Germany.

Email:

Vivien.kmietczyk@med.uni-heidelberg.de

mirko.voelkers@med.uni-heidelberg.de

Word Count: 7697 (introduction to figure legends)

Abstract

Background:

The structure and function of cardiomyocytes rely on tightly regulated gene networks that control development, maturation, and homeostasis. Disruption of these networks is associated with cardiomyopathies such as hypertrophic and dilated cardiomyopathy, leading to heart failure. Our previous work identified the transcription factor “Zinc Finger E-Box Binding Homeobox 1” (ZEB1) as a downstream effector of Cytoplasmic Polyadenylation Element Binding Protein 4 (CPEB4), an RNA-binding protein responsive to cardiac stress. While ZEB1 is known for its role in cancer metastasis and epithelial-to-mesenchymal transition (EMT), its function in cardiomyocytes is not well understood. Based on previous findings, we hypothesize that ZEB1 is essential for maintaining the structural integrity and contractile function of cardiomyocytes.

Hypothesis and objectives:

We hypothesized that ZEB1 plays a critical role in maintaining cardiomyocyte structure and function. Deletion of Zeb1 may result in sarcomeric disorganization and mitochondrial dysfunction, whereas its overexpression appears to promote maladaptive hypertrophy. Our objectives are to:

1. Investigate if ZEB1 overexpression induces pathological cardiac remodeling.
2. Examine the effects of ZEB1 deletion on cardiomyocyte structure and function.
3. Identify ZEB1-regulated transcriptional networks.

Methods:

AAV9-Zeb1 was used for the overexpression of Zeb1. Using a myosin heavy chain alpha (αMHC) Cre system, we created a Zeb1 conditional knockout mouse. To evaluate the cardiac function, we used methods like echocardiography, electron microscopy, immunohistochemistry. We identified differential expressed genes upon deletion of Zeb1 using RNA-seq and integrated the data set with ChIP-seq.

Results:

ZEB1 deletion leads to sarcomere damage, mitochondrial dysfunction, and dedifferentiation, with more pronounced effects in females. Overexpression promotes hypertrophic remodeling. Echocardiographic analysis showed progressive systolic dysfunction, and histology revealed sarcomeric disarray, again especially in females. A tamoxifen-inducible ZEB1 knockout mouse model confirmed ZEB1's crucial role in fully differentiated cardiomyocytes.

Conclusions:

ZEB1 is critical for cardiomyocyte homeostasis, and maintaining its function is necessary for normal cardiac performance and structure.

Condensed Abstract

We identified Zeb1 as a downstream target of Cpeb4 in cardiac hypertrophy. While ZEB1's role in cancer and EMT is known, its impact on cardiomyocytes remains largely underexplored. We hypothesize that ZEB1 regulates cardiomyocyte maturation and function, which is crucial for structural integrity and contractility. Zeb1 deletion disrupts sarcomeric organization and induces cardiac dysfunction, notably more severe in females. RNA sequencing confirms that ZEB1 loss in females increases the expression of epithelial and extracellular matrix (ECM) genes. ZEB1's overexpression induces pathological hypertrophy and progressive cardiac dysfunction. These findings underscore ZEB1's critical role in cardiac structure and function, further increasing our understanding of gene regulatory networks in cardiomyocytes.

Key words: ZEB1; cardiac remodeling; dilated cardiomyopathy; sarcomeric integrity; heart failure; Mitochondrial defect

Abbreviation list:

1. ZEB1 – Zinc finger E-box-binding homeobox 1
2. TAC – Transverse Aortic Constriction
3. DCM – Dilated Cardiomyopathy
4. HCM – Hypertrophic Cardiomyopathy
5. NRCMs – Neonatal Rat Cardiomyocytes
6. PE – Phenylephrine
7. AAV9 – Adeno-Associated Virus serotype 9
8. cKO – Conditional Knockout

9. icKO – Inducible Conditional Knockout
10. EF – Ejection Fraction

Introduction

ZEB1: A Context-Dependent Transcriptional Repressor

Cardiomyocytes are the contractile cells of the heart, originating from mesodermal progenitors and undergoing tightly regulated differentiation and maturation processes (1–4). Disruptions in cardiomyocyte homeostasis cause various heart diseases, including hypertrophic and dilated cardiomyopathy, which significantly contribute to global heart failure and mortality (5–9).

The transcriptional repressor zinc finger E-box binding homeobox 1 (ZEB1) is primarily known for its function in the EMT (5,6), which is essential for development, wound healing, and the proliferation of cancer cells (6–10). To facilitate cellular plasticity and mobility, ZEB1 suppresses epithelial markers like E-cadherin (*Cdh1*) and increases the expression of mesenchymal genes like N-Cadherin (*Cdh2*) (11,12). In skeletal muscle, Zeb1 preserves the mesenchymal identity of satellite cells and is crucial for effective muscle repair (13). Previous research on Zeb1 have primarily focused on its functions in cancer biology (14–16), stem cell maintenance (17), tissue fibrosis (18,19), and regeneration (13). Functional genomic studies in murine models have demonstrated that ZEB1 is indispensable for early mesendodermal differentiation (17,20,21), including cardiovascular lineage specification (22). Knockout studies in mice show that loss of ZEB1 leads to complex developmental defects, including sporadic vascular changes and hemorrhages, indicating a role in vascular and cardiac development (23). ZEB1, together with co-factors like HDAC2, works as a key regulator of vascular tone and cardiovascular

health (22). Reduced ZEB1 levels activate these genes, altering differentiation pathways relevant to the heart and vasculature.

We recently performed a comprehensive proteome-wide screen to identify RNA-binding proteins (RBPs) and translationally regulated mRNAs associated with pathological cardiomyocyte growth. This investigation revealed that the *Zeb1* transcript undergoes post-transcriptional regulation mediated by specific RBPs. Notably, elevated Zeb1 protein expression, in the absence of corresponding changes in mRNA levels, is dependent on the activity of specific RBPs and pressure overload induced heart failure is associated with increased protein levels of Zeb1. Still the function of Zeb1 in adult cardiac myocytes and its involvement in pathological remodeling remains unexplored.

Rationale and Significance

Given ZEB1's emerging role as a regulator of mesenchymal identity (5,7,24), its influence on cardiomyocyte structure and gene networks critical for cardiac function (21–24), we hypothesize that ZEB1 acts as a master regulator of cardiomyocyte structure.

6. Materials and Methods

Isolation of neonatal rat cardiomyocytes

Neonatal rat cardiomyocytes (NRCM) were isolated from 1–3-day-old Wistar rats by enzymatic digestion of ventricles. After pre-plating to remove noncardiomyocytes, cells were plated at 50,000 cells/cm² on gelatin-coated plates and maintained at 37 °C, 5% CO_2. Experiments were performed the following day.

Adenovirus and AAV9 production and viral transduction

ZEB1 entry clones (pDONR221, NM_011546.3) were subcloned into pAd/CMV/V5-DEST via Gateway LR reaction. Constructs were transformed into E. coli, verified by Sanger sequencing, and used to produce adenoviruses in HEK293A cells. AAV9 vectors were produced via PEI transfection in 50 T175 HEK293T flasks using helper and ITR plasmids.

Immunoblotting

Protein concentration was measured by Bio-Rad DC assay after RIPA lysis. Samples were mixed with Laemmli buffer, heated, separated by SDS-PAGE, transferred to PVDF membranes, blocked, incubated with primary and secondary antibodies, and visualized using ECL detection.

Table. 1 Antibodies used in western blot.

Target	**Species**	**Dilution**	**Supplier**	**Catalog number**
Zeb1	Rabbit	1:1000	Thermo Scientific	703354
B-Tubulin	Rabbit	1:1000	Abcam	Ab6046

Actin	Mouse	1:1000	Santa Cruz Biotechnology	sc-8432
E Cadherin	Rabbit	1:1000	Proteintech	20874-1-AP
Cytokeratin 8	Rabbit	1:1000	Proteintech	27105-1-AP
Peroxidase-AffiniPure Anti-Mouse	donkey	1:5000	Jackson Immuno Research	715035151
Peroxidase-AffiniPure Anti-Rabbit	Goat	1:5000	Jackson Immuno Research	111035144

RNA isolation and quantitative RT-PCR

Total RNA from NRCMs and homogenized. Snap-frozen tissues in RIPA buffer were isolated using Qiazol with chloroform/isopropanol precipitation. cDNA was synthesized using the iScript Kit, and qRT-PCR was performed with SYBR Green and 3μM primers. Relative expression was calculated using the ΔΔCT method with 18s or HPRT.

Table. 2 List of primers

Antibody	**FOR**	**REV**
Mouse and Rat 18s	CGA GCC GCC TGG ATA CC	CAT GGC CTC AGT TCC GAA AA
Mouse *Hprt*	GGGGCTGTACTGCTTAACCAG	TCAGTCAACGGGGGACATAAA
Rat *Nppa*	GGAGCAAATCCTGTGTACAGTG	ACCTCATCTTCTACCGGCAT
Rat *Nppb*	GCAGCATGGATCTCCAGAAGG	CTGCAGCCAGGAGGTCTTCC
Mouse *Nppa*	TTG TGG TGT GTC ACG CAG CT	TGT TCA CCA CGC CAC AGT G
Mouse *Nppb*	TCC TAG CCA GTC TCC AGA GCA A	GGT CCT TCA AGA GCT CTG TCT G
Mouse *Zeb1*	ATT CAG CTA CTG TCA GCC CTG C	CAT TCT GGT CCT CCA CAG TGG A

Mouse *Zeb2*	GAG CAG GTA ACC GCA AGT TC	AAG CGT TTC TTG CAG TTT GG
Rat *Myh6*	TAA CCG GAG TTT AAG AGT GAC AGG	TAG GCG CTC CTT CTC TGA CT
Mouse *Myh6*	GCA AAG GAG GCA AGA AGA AAG G	TGA GGG TGG GTG GTC TTC AG

Immunofluorescence and staining

Immunofluorescence was performed on NRCMs to assess cell size. Cells were fixed with 4% PFA, permeabilized, and blocked with 10% horse serum. Primary antibodies were applied overnight at 4°C, followed by secondary antibodies and DAPI staining. Images were captured using a Leica SP8 confocal microscope. Cell size was quantified using Fiji (ImageJ) through manual measurements.

Table. 3 Antibodies used for immunofluorescence.

Target	**Species**	**Dilution**	**Supplier**	**Catalog number**
Zeb1	Rabbit	1:100	Thermo Scientific	703354
Sarcomeric Actinin	Mouse	1:1000	Santa Cruz Biotechnology	sc-8432
CSRP3	Rabbit	1:1000	Proteintech	10721-1-AP
Wheat Germ Agglutinin, FITC conjugate		1:50	Sigma-Aldrich	L4895-2MG
Anti-rabbit IgG-FITC	Donkey	1:100	Jackson Immuno Research	711-095-152
Anti-rabbit IgG-Cy3	Donkey	1:100	Jackson Immuno Research	711-165-152
Anti-Mouse IgG-FITC	Donkey	1:100	Jackson Immuno Research	715-095-151
Anti-Mouse IgG-Cy3	Donkey	1:100	Jackson Immuno Research	715-165-151

Animal Model

All animal procedures were approved by the Baden-Württemberg council (Approval: G-190/21) and conducted in accordance with animal welfare regulations. Floxed *Zeb1* knockout (ZEB1 KO) mice on a C57BL/6N background were generated in the laboratory of Prof. Dr. Thomas Brabletz at the Clinical Molecular Biology Research Center (KMFZ), Friedrich-Alexander University Erlangen-Nuremberg (25). Zeb1cKO mice were crossed with the MerCreMer WT line to generate a tamoxifen-inducible Zeb1 cKO model. Mice were bred and housed in Heidelberg's central animal facility under controlled temperature and humidity, with a 12:12 hour light-dark cycle, and provided ad libitum access to standard chow.

Echocardiography

Echocardiography was performed using the Visual Sonics Vevo F2 system with a UHF46x transducer. B-mode and M-mode images were captured from parasternal long and short axes. Mice were anesthetized with 1.5% isoflurane on a 37°C heated plate. Heart function was analyzed at 350–500 bpm using VevoLab 5.9.0 software.

Electron microscopy

Heart tissue was fixed in glutaraldehyde/paraformaldehyde, post-fixed with osmium tetroxide, stained with uranyl acetate, dehydrated, and embedded in Spurr resin. Ultrathin 70 nm sections were contrast-stained and imaged in the Electron Microscopy Core Facility (EMCF) at the Heidelberg University using a JEOL JEM-1400 TEM at 80 kV, 8kX–10kX magnification.

Staining of Mouse Heart Tissue for Morphological Analysis

Mice were euthanized and hearts arrested in diastole using $CdCl_2$. After PBS perfusion and formalin fixation, hearts were paraffin-embedded. Sections (4–5μm) underwent H&E, Masson's Trichrome, or immunofluorescence staining. Following antigen retrieval, primary and secondary antibodies were applied. DAPI-stained sections were imaged using a Leica SP8 confocal microscope.

Isolation of adult mouse cardiomyocytes (AMCM)

Adult cardiomyocytes from 8-week ZEB1KO and WT mice were isolated using a Langendorff-free method (26). Hearts were perfused with EDTA, perfusion, and collagenase buffers, then minced and dissociated. Digestion was stopped, cells filtered, calcium gradually reintroduced, and cardiomyocytes plated (~50,000cells/cm²) on laminin-coated plates for culture.

Bulk RNA seq

Total RNA from left ventricular tissue was extracted using TRIzol and RIPA homogenization. RNA quality (RIN>7) was confirmed via NanoDrop and Bioanalyzer. mRNA libraries were prepared with NEBNext Ultra II and sequenced (150bp paired-end) on Illumina NovaSeq. Paired-end, rRNA-depleted sequencing data were analyzed following quality control. Low-quality regions and adapter sequences were removed using Flexbar (27), and residual rRNA reads were filtered with Bowtie2 (28) using an rRNA-specific index. Reads were aligned to the ENSEMBL mouse genome build 107 (mm39) using STAR (29), and gene-level counts were obtained with Rsubread (30). Quality

metrics and mapping summaries were assessed via MultiQC (31). Differential expression was analyzed with edgeR (32). GO analysis was performed with topGO, using genes with RPKM≥1 across all samples as background. Heatmaps were generated using Complex Heatmap (33). All downstream analyses were conducted in R. Sequencing raw data is available under accession number SRP630684 in the SRA, processed gene counts are available in GEO under accession number GSMXXXXX.

Chromatin immunoprecipitation Sequencing

NRCMs were crosslinked (40 million cells, 1% formaldehyde for 10min), quenched (250mM glycine), washed with PBS, and the nuclei were isolated. Chromatin was sonicated (3×15 cycles, Bioruptor) and cleared as described earlier (34). ChIP was performed using ZEB1 antibody, we used 4µg of the antibody for the pulldown.

ChIP samples were treated with RNase A, Proteinase K, and SDS overnight. DNA was purified (phenol/chloroform), libraries prepared according to the manufactures' protocols (NEBNext Ultra II) and quality-checked on TapeStation. Sequencing was performed on a DNBSEQ-G400 platform.

FASTQ data were annotated to the rat genome (rn7) using bowtie2 (version2.5.2). Only uniquely mappable reads have been subjected to further analysis. The resulting BAM files have been used for MACS (Model based analysis of ChIP-seq) peak calling (Version2.2.6) with a selected q-value (false discovery rate) of 0.05 and normalized to the corresponding input file. The DeNovo transcription factor analysis of called peaks with promoter peak was done in HOMER (version5.1) using the size given option and randomly selected background sequences.

For illustrations, bigwig files were generated via bamCoverage (version3.5.5) in Reads Per Kilobase per Million (RPKM) and 50 bp binning and averaged using bigwigAverage (version3.5.5).

The heatmaps shown were built with deeptools (version3.5.4) via usegalaxy.org (35) using a bed file of either all differentially regulated transcripts from the RNA-seq or a bed file of all summarized peaks from the single replicates of the ChIP-seq. The enrichment shown is averaged from the three replicates. Single exemplary ChIP-seq tracks of Input and pulldown are shown in Suppl.Figure.7. Peak annotation was done with HOMER (version5.1). Promoter peaks were defined as -500bps to +100bps relatively to the transcriptional start site (TSS).

The number of reads, the percentage of uniquely mappable reads and the amount of called peaks are listed separately. Raw and annotated data have been submitted to the EMBL-EBI database (accession number: E-MTAB-15712).

Table. 4 Antibodies used for Immunoprecipitation.

Target	**Species**	**Supplier**	**Catalog number**
Zeb1	Rabbit	Thermo Scientific	703354
(DA1E) mAb IgG XP®	Rabbit	Cell Signalling Technology	D2A11
Dynabeads Anti-Rabbit IgG	Sheep	Thermo Fisher Scientific	11203D

Results

Regulation of ZEB1 protein expression in cardiac hypertrophy and cardiomyopathy models.

To test the hypothesis that upregulation of Zeb1 expression is a common response in the heart to stress stimuli, the expression of Zeb1 in different mouse models of heart failure as well as in human heart failure samples (Procured by the local authorities, Ethics approval number: S-390/2011) was checked at protein levels. Significant reduction in ZEB1 protein levels was observed in both ischemic cardiomyopathy (ICM) ($p=0.0008$) and dilated cardiomyopathy (DCM) ($p=0.0018$) as compared to non-failing (NF) heart samples (Fig.1a). We observed a significant elevation ($p=0.001$) in ZEB1 protein levels in heart lysates of left ventricles (LV) in Mybpc3 knockout mice (Fig.1b), a mouse model of genetic hypertrophic cardiomyopathy (HCM) (36). Conversely, in Rbm20 knockout mice exhibiting dilated cardiomyopathy (DCM) (37), we observed a reduction ($p=0.16$) in ZEB1 protein levels (Fig.1c).

Zeb1 overexpression induces cardiomyocyte hypertrophy and cardiac dysfunction *in vitro* and *in vivo*.

We used an adenovirus-mediated overexpression approach in neonatal rat cardiomyocytes (NRCMs) to mimic increased Zeb1 expression observed after HCM (Fig.2a). To determine how Zeb1 overexpression affects hypertrophic responses, the α1-adrenergic receptor agonist phenylephrine (PE) was administered to both the control and Zeb1-overexpressing (Zeb1OE) NRCMs. Increased ZEB1 levels following PE treatment was confirmed by western blot and qRT-PCR ($p<0.0001$) (Fig.2a,b). NRCMs

overexpressing Zeb1 with and without PE treatment (Fig.2c) showed a significant increase ($p<0.002$) in cell size with Zeb1OE (Fig.2d). Accordingly, NRCMs overexpressing Zeb1 displayed increased ($p=0.001$) expression of the hypertrophic markers *Nppa* (and *Nppb*, Supp.Fig.1a) in Zeb1OE NRCMs in combination with the reduction ($p<0.0001$) of *Myh6*, comparable to PE-treated cells (Fig.2e).

To validate the functional effect of Zeb1 *in vivo,* we used an Adeno-Associated Virus 9 (AAV9) cardiomyocyte-specific Zeb1 vector. Recombinant AAV9 particles were created, purified, and systemically injected into the tail veins of 8-week-old male (Fig.2f) and female (Supp.Fig.2b,c,d,e) mice. Increased Zeb1 expression was validated by western blot (Fig.2g), qRT-PCR ($p<0.0001$) (Supp.Fig.2f), and immunostaining of left ventricle tissue sections (Fig.2h).

Echocardiographic assessment showed that at week seven after the AAV9 injection, the ejection fraction of the Zeb1OE mice was significantly ($p=0.001$) decreased, and the left Ventricular Posterior Wall thickness during diastole (LVPW;d) was increased ($p=0.036$), (Fig.2i). Though the heart weight to body weight ratio remained unchanged (Fig.2j), the cardiomyocyte cross-sectional area upon Zeb1OE, as quantified by WGA staining, showed increased cardiomyocyte size ($p<0.0001$) (Supp.Fig.2g) and expression of typical hypertrophic markers such as *Nppa* ($p=0.001$) and *Nppb* ($p=0.02$) were significantly increased in the left ventricle tissue lysates of Zeb1OE hearts as compared to control hearts (Fig.2k). To assess fibrosis in Zeb1OE mice, Masson's Trichrome Staining of left ventricle tissue sections was performed and significant differences ($p=0.005$) were observed in Zeb1OE tissue sections compared to control animals (Supp.Fig.2h). In summary, Zeb1 gain-of-function leads to cardiac dysfunction and hypertrophy.

Cardiomyocyte-specific deletion of Zeb1 leads to progressive cardiac dysfunction and pathological remodeling.

We used the αMHC-Cre mouse model to create a cardiomyocyte-specific Zeb1 conditional knockout (cKO) mouse model (25) (Fig.3a). Cardiomyocyte-specific Zeb1 deletion was validated by western blot ($p=0.004$) and immunostaining of left ventricular tissue, comparing the Zeb1 expression in left ventricular tissue and liver lysates of Zeb1cKO and WT adult mice (Fig.3a,b, Supp.Fig. 3a).

Echocardiography was performed to assess cardiac function and cardiac parameters of 12-week-old and 25 weeks and older mice. As early as 12 weeks of age, Zeb1cKO mice showed a significant decrease ($p=0.0006$) in systolic heart function, with an average Ejection Fraction (EF) of about 40% compared to 60% in WT mice (Fig.3c,d.). The diastolic LV volume ($p=0.003$) and LV diameter ($p=0.015$) were significantly increased in 12-week-old male mice (Fig.3d). In older Zeb1cKO mice (≥25 weeks), the condition worsened, with the EF of Zeb1cKO mice decreasing to 20% ($p<0.0001$) (Fig.3d).

Accordingly, histological analysis confirmed wall thinning and dilation of the left ventricle of Zeb1cKO mice (Fig.3e), while overall heart weight to body weight ratio was not altered (Fig.3f). Pathological remodeling in the adult Zeb1cKO was assessed by qRT-PCR of the remodeling markers *Nppa* ($p<0.0001$) and *Nppb* ($p<0.0001$), which revealed higher transcriptional levels in Zeb1cKO LV lysates compared to WT (Fig.3g). We did not see any change in the mRNA levels of Zeb2 (Zeb1's closest homolog) in the absence of Zeb1, both in young and old mice (Supp.Fig.3b), indicating that Zeb1 plays a non-redundant role in maintaining cardiac homeostasis.

Female Zeb1cKO mice develop a severe dilated cardiomyopathy phenotype and adult-onset Zeb1 deletion causes cardiac dysfunction.

Female Zeb1cKO mice exhibited a more pronounced cardiac phenotype compared to males. By 20 weeks of age, mortality began to increase among female Zeb1cKO mice, with only 80% surviving to 30 weeks (Fig.4a), whereas 95% of male cKO mice reached the same age (Supp.Fig.3c). Hearts of female Zeb1cKO also had severely dilated ventricles assessed by echocardiography (Fig.4b). Severe remodeling was also reflected by echocardiographic measurement showing a significant decrease in EF down to 8–10% ($p<0.0001$), and a significant increase in the ventricular volume ($p=0.02$) and diameter ($p=0.031$) of Zeb1cKO 25 weeks and older females (Fig.4c). The heart weight to body weight ratio was increased ($p=0.047$) in older female mice (Fig.4d) and Masson's Trichrome stained histological sections confirmed dilation of both right and left ventricles in Zeb1cKO mice (Fig.4e). The pathological remodeling markers *Nppa* ($p<0.0001$) and *Nppb* ($p=0.0003$) were significantly higher in female Zeb1cKO LV lysates compared to WT (Fig.4f). The cardiomyocyte cross-sectional area of older female Zeb1cKO mice, as quantified by WGA staining, showed increased cardiomyocyte size ($p<0.0001$) (Supp.Fig.3d). We conclude that ZEB1 is essential for maintaining cardiac integrity and deletion causes dilatation of the heart with a more severe phenotype in female mice compared to male.

However, the cardiomyocyte-specific KO model used in this study relies on the Zeb1 deletion in the late embryonic stage because of the Cre recombinase expression under the αMHC promoter, whose activity rises perinatally (Supp.Fig.3e,f). We confirmed the knockout of Zeb1 in the postnatal day-2 (P2) hearts as compared to the embryonic day

14 (E14) hearts, where Zeb1 was still expressed in the Zeb1cKO strain (Supp.Fig.3g). Previous research suggested an impact of Zeb1 on proliferation of neonatal cardiomyocyte (38). Consequently, we analyzed the expression of proliferation markers in embryonic and postnatal cardiomyocytes by Ki67 staining of sections of wild type and of Zeb1cKO mice. Zeb1cKO led to a significant decrease (p=0.001) of Ki67-positive cells in P2 hearts as compared to E14 hearts (Supp.Fig. 3h,i,j).

Hence, the cardiac dysfunction and severe heart failure of Zeb1cKO mice could at least partially result from Zeb1 deletion in the late perinatal stage, causing dysfunctional maturation or proliferation of cardiomyocytes.

Temporal deletion of Zeb1 in mature cardiomyocytes reveals loss of cardiac function in adult heart

To further evaluate the role of Zeb1 in adult cardiomyocytes, we created an inducible Zeb1 conditional knockout (icKO) mouse model exclusive to cardiomyocytes, using a MERCreMER recombinase system regulated by the αMHC promoter (Fig.4g). The knockout was confirmed in adult cardiomyocytes by western blot (p=0.037) (Fig.4g). Echocardiography showed, that seven weeks after ZEB1KO induction, the left ventricular EF was not altered in male Zeb1icKO mice (Supp.Fig.4a,b,c) whereas cardiac function of female Zeb1icKO mice, was significantly decreased (p=0.0003) (Fig.4h,i), while the heart weight to body weight ratio and the LV volume and diameter remain unchanged (Fig.4j). There was no noticeable reduction in the left ventricular wall thickness of the female Zeb1icKO mice as compared to WT as evident from the Masson's Trichrome stained heart sections (Supp.Fig.4d).

In summary, both perinatal and adult depletion of ZEB1 deteriorates heart function and structure, inducing a dilated phenotype which is accompanied with cardiac dysfunction.

Zeb1 deletion disrupts sarcomeric architecture in cardiomyocytes

The analysis of the phenotype of Zeb1cKO mouse hearts showed functional impairment indicating structural dysfunction induced by Zeb1 deletion. To confirm structural changes in cardiomyocyte architecture that might cause cardiac dysfunction and dilation in Zeb1cKO mice, we used Transmission Electron Microscopy (TEM) on heart tissue from WT and Zeb1cKO female mice. Significant sarcomeric disarray, as evidenced by a total loss of actin and myosin filament integrity, was discovered by TEM (Fig.5a).

Given the TEM findings, we further postulated that Zeb1 deletion modifies sarcomere structure. To objectively evaluate these alterations, sarcomere dimensions were measured in electron microscopy images ($p=0.022$) (Fig.5b) as well as in isolated cardiomyocytes from WT and Zeb1cKO mice using the Ionoptix system (Fig.5c). ACMs from Zeb1cKO showed a notable increase ($p=0.0008$) in sarcomere length compared to those from WT hearts (Fig.5c,d). To validate these findings in older animals, cardiomyocytes were isolated from formaldehyde-fixed frozen cardiac tissue (39) from both male and female 25 weeks. The length-to-width ratio was calculated, showing a significant decrease ($p<0.0001$) in Zeb1cKO (Supp.Fig.5a) and we performed immunostainings for the Z-disc-associated protein MLP (Muscle LIM Protein) on cardiac sections of female mice (Fig.5e), showing a notable increase ($p=0.0003$) in sarcomere length (Fig.5f) and Z-disc thickness ($p=0.003$) (Fig.5g) in female Zeb1cKO mice, compared to malecKO mice. Sarcomere length and Z-disc thickness of Zeb1icKO heart

sections were also evaluated by MLP2-immunostainings. Male hearts showed no discernible alterations (Supp.Fig.5b,c), while female Zeb1icKO hearts (Fig.5h) showed a significant increase in both sarcomere length (p=0.12) (Fig.5i) and Z-disc thickness (p=0.008) (Fig.5j), thereby suggesting an important role of ZEB1 in adult CM function.

Bulk RNA-Seq and *de novo* motif analysis identify Zeb1 as a key transcriptional repressor of epithelial gene programs in female cardiomyocytes

As Zeb1 functions as a transcription co-regulator, phenotypic and molecular analysis was carried out to assess gene expression differences resulting from Zeb1 deficiency in female mice. Bulk RNA sequencing was performed on left ventricle tissue from female WT and Zeb1cKO mice (Fig.6a). Gene Ontology (GO) term enrichment analysis identified a subset of differentially expressed genes (DEGs), predominantly associated with extracellular matrix and epithelial genes in the upregulated gene subset (Fig.6b). The downregulated DEGs were enriched for genes involved in cardiac contraction (Supp.Fig.6a).

A comprehensive *de novo* motif analysis using the HOMER v4.11 algorithm was performed on the transcriptomes of Zeb1cKO and WT mice. This analysis revealed that the ZEB1 binding motif was the top-ranked motif enriched in the promoters of DEGs, suggesting a strong likelihood of direct transcriptional regulation by ZEB1 (Fig.6c). Specifically, among the 1,396 upregulated DEGs in female ZEB1cKO mice, 295 (3.67%) genes contained a known ZEB1 binding motif in their promoter regions. In contrast, only 96 (1.34%) out of 702 downregulated DEGs harbored a ZEB1 motif (Fig.6d,e). These findings align with the known function of ZEB1 as a transcriptional repressor.

Among the upregulated DEGs in female Zeb1cKO vs. WT mice, we found Cdh1 ($p<0.0001$) and Krt8 (Cytokeratin 8) ($p<0.0001$) as major epithelial markers (Fig.6f) among other genes like Prom2 and Cldn7 (Supp.Fig.6b). Correspondingly, protein levels of these markers were elevated in Zeb1cKO LV tissue lysates and adult mouse cardiomyocytes (Fig.6g).

Integration of Zeb1 ChIP-seq and Transcriptomics Reveals Direct Regulatory Programs in Cardiomyocytes

With the aim to identify direct cardiomyocyte specific target genes, we performed Zeb1 ChIP-seq on neonatal rat ventricular cardiomyocytes for the ChIP-seq because of higher Zeb1 expression level compared to adult cardiomyocytes (Supp.Fig.7a) and a higher chromatin yield (Fig.7a).

Principal component analysis (PCA) was performed on the ChIP-seq datasets to assess sample variability and overall data quality. The input samples clustered tightly together, indicating high reproducibility of the control datasets. Similarly, the three immunoprecipitated (IP) samples also grouped closely, but were clearly separated from the input samples along the first principal component, reflecting distinct enrichment patterns captured by the ChIP (Supp.Fig.7b).

Of 71,907 annotated peaks about 12,800 are localized at exonic regions (17.8%), about 40,000 (55.2%) in intronic regions and 8,146 in intergenic regions (11.3%). Approximately 8,648 (12%) of peaks from Zeb1 immunoprecipitated chromatin mapped to the Transcription Start Site (TSS) or the promoter region with the promoter peaks having the biggest mean size (Fig.7b).

To examine the genome-wide distribution of Zeb1 associated chromatin binding, we visualized Input-normalized ChIP-seq read density across all annotated genes. Heatmaps and averaged density profiles revealed enrichment of Zeb1 at gene promoters, with signal peaking around the TSS. When analysis was restricted to genes with ChIP-seq peaks detected within promoter regions, a sharper enrichment profile can be observed, supporting preferential binding of Zeb1 at promoter-proximal regions (Fig.7c,d). GO enrichment analysis of these genes revealed that ZEB1 associates with genes in diverse biological processes like several metabolic processes and cellular response to stress (Fig.7e).

We further integrated Zeb1-chromatin binding with differentially expressed transcripts. Zeb1 enrichment is seen e.g. at the promoter region of Cdh1, which is a known Zeb1 target. Another example would be Krt8 with distinct Zeb1 binding in the promoter region (Fig.7f). To identify putative direct Zeb1 targets in a genome-wide manner, we compared all genes with Zeb1-binding in the promoter region to differentially expressed genes from our RNA-seq dataset of female Zeb1cKO mice and to genes containing a predicted Zeb1 motif identified by HOMER analysis within the DEGs. The Venn diagram illustrates the overlap among these datasets, highlighting the subset of genes that are both differentially expressed and promoter-bound by Zeb1 with an associated motif, representing high-confidence primary Zeb1 targets (Fig.7g). The heatmap (Supp. Fig.7d) and averaged density profiles of these 246 genes promoter-bound by Zeb1 with an associated motif, have a sharper peak before the TSS (Fig.7h).

Interestingly, we identified 567 genes that were both bound by Zeb1 at their promoters (ChIP-seq) and differentially expressed (RNA-seq), but in which HOMER motif analysis

of the DEGs did not detect Zeb1 motifs. These genes may represent novel or non-canonical Zeb1 targets that were not predicted based on motif enrichment alone. However, peaks could also result from Co-immunoprecipitation of other transcription factors, without actual binding of Zeb1 to the predicted DNA binding motif. The heatmaps (Supp.Fig.7d) and averaged density profiles of these 567 genes revealed enrichment of Zeb1 at promoter region, with signal peaking before the TSS, very similar to the Zeb1 motif genes identified by RNA-seq (Fig.7h).

The expression of these 567 intersecting genes was downregulated in 171 genes whereas upregulated for 396 (Fig.7i). Gene ontology analysis of upregulated genes showed similar enrichment in cellular components of the extracellular matrix and the plasma membrane (Supp.Fig.7e), like all genes with a peak in the promoter region. Downregulated genes with a ChIP-seq peak enriched for genes of cellular components of mitochondria, with highest count of genes and lowest FDR of $p<0.00001$ (Fig.7j). The detailed look into the ChIP-seq analysis of the mitochondrial genes Acaa2 (Acetyl-CoA Acyltransferase 2) and Smim20 (small integral membrane protein 20) revealed sharp peaks precisely at transcription start sites. (Fig.7k). *Acaa2* and *Smim20* are significantly downregulated ($p<0.001$ and $p<0.005$) in Zeb1cKO mice, indicating that Zeb1 usually induces its expression, rather than acting as transcription repressor.

Zeb1 regulates mitochondrial component expression

Integrative RNA- and ChIP-seq suggest a direct Zeb1-dependent regulation of expression of mitochondrial genes. Additionally, taking a closer look into our TEM pictures, we

observed mitochondrial abnormalities in Zeb1cKO, which included structural disruption and a reduced number of mitochondria (Fig.8a). The quantification of mitochondrial DNA in hearts of Zeb1cKO and WT mice showed reduction of mitochondrial vs genomic DNA, by qRT-PCR ($p<0.0001$), confirming the loss of mitochondria (Fig.8b).

We performed Seahorse assays on NRCMs depleted for Zeb1 by siRNA to functionally assess how the consequential loss of mitochondrial component genes and the reduced number of mitochondria impact cellular bioenergetics. Transcriptomic data indicated downregulation of several key mitochondrial genes, including Acaa2, which is required for fatty acid β-oxidation, and Smim20, a factor critical for complex IV assembly and stability. Given these molecular changes, we expected a reduction in oxygen consumption rate (OCR), reflecting impaired oxidative phosphorylation capacity.

Indeed, seahorse assay revealed that knockdown (KD) cells exhibited significantly reduced mitochondrial respiration compared to controls (Fig.8c). Under basal conditions, OCR was modestly decreased in Zeb1KD cells (Fig.8d), but the impairment became significantly reduced ($p=0.02$) following FCCP treatment, where maximal respiration reached only ~300 pmol/min compared to ~450 pmol/min in controls (Fig.8e). This reduction in maximal capacity reflects a loss of spare respiratory capacity in the KD cells. These results demonstrate that knockdown of Zeb1 leads to compromised oxidative phosphorylation efficiency, presumably by direct downregulation of mitochondrial components.

Discussion

This study uncovers a previously unrecognized and critical role of the transcription factor ZEB1 in regulating cardiac structure and function, with potential implications for both hypertrophic and dilated cardiomyopathy. Our findings demonstrate that Zeb1 expression is tightly regulated at the translational level during cardiac stress and disease, and that both gain and loss of Zeb1 function led to profound and distinct forms of cardiac remodeling. Notably, we found no evidence of compensatory upregulation of Zeb2, the closest homolog of Zeb1, in either young or aged Zeb1cKO hearts. Despite sharing similar zinc finger and homeodomain structures and overlapping roles in other systems, such as during EMT and neural development, Zeb2 does not appear to compensate for the loss of Zeb1 in cardiomyocytes (40,41).

In mice models of genetic HCM (Mybpc3 KO) mouse, ZEB1 protein levels are upregulated independently of mRNA changes, highlighting a post-transcriptional regulatory mechanism. Conversely, ZEB1 levels are reduced in the ICM and DCM human patient samples and in mice models of DCM (Rbm20 KO). These findings indicate that ZEB1 protein levels could act as a molecular sensor and regulator in cardiomyopathies.

Overexpression of Zeb1 in cardiomyocytes, both *in vitro* and *in vivo*, recapitulates key features of hypertrophy, including increased cardiomyocyte size, upregulation of fetal gene markers (e.g., *Nppa, Nppb*), and compromised cardiac function. The observation that sustained cardiomyocyte-specific Zeb1 overexpression in mice reduces ejection fraction and induces wall thickening, fibrosis, and sarcomeric disarray underscores its

pathogenic potential when dysregulated. These findings are consistent with a role for Zeb1 in driving maladaptive cardiac remodeling (13).

While increased Zeb1 expression causes hypertrophy in mice, cardiomyocyte-specific deletion of Zeb1 leads to progressive cardiac dilation and dysfunction, with severe systolic impairment and chamber dilation. Interestingly, these effects are more severe in female mice, where a significant portion of Zeb1cKO females die within 30 weeks of age. Structural analysis reveals extensive sarcomeric disorganization and mitochondrial abnormalities in ZEB1-deficient hearts, implicating Zeb1 in the maintenance of both sarcomere integrity and cardiomyocyte energetics. This is in line with the know function of Zeb1 for the induction of mesenchymal genes (13,19,21).

Importantly, our inducible knockout model reveals that deletion of Zeb1 in mature cardiomyocytes does not lead to cardiac dysfunction in males, but induces sarcomeric disarray and impaired function in females. These results might suggest a sex-specific sensitivity to Zeb1 loss and Zeb1 function might be beyond development in the ongoing maintenance of cardiomyocyte architecture in female adulthood.

Mechanistically, RNA-seq analysis of Zeb1-deficient hearts discovered a prominent upregulation of epithelial gene signatures, including *Cdh1* and *Krt8*, consistent with a reversal of Zeb1's canonical role in repressing epithelial genes during/after EMT. Motif enrichment analysis further supports a direct transcriptional role for Zeb1 in maintaining cardiomyocyte identity by repressing epithelial and extracellular matrix genes. The disproportionate enrichment of Zeb1 motifs among upregulated genes confirms Zeb1's function primarily as a transcriptional repressor in the heart.

Our integrative analysis of Zeb1 ChIP-seq and transcriptomics in cardiomyocytes demonstrates that Zeb1 preferentially binds promoter-proximal regions, where it promotes expression of genes that are components of mitochondria. The identification of high-confidence targets with both promoter binding and motif enrichment supports a direct regulatory role of Zeb1, while the larger set of promoter-bound DEGs lacking canonical motifs suggests non-canonical binding or co-factor–mediated recruitment. Importantly, the downregulation of mitochondrial genes such as Acaa2 and Smim20 in Zeb1cKO mice highlights Zeb1 as a critical regulator of metabolic and structural programs in cardiomyocytes. Mitochondrial loss, ultrastructural abnormalities, and decreased oxygen consumption rates further implicate Zeb1 in maintaining the metabolic and energetic integrity of cardiomyocytes.

Collectively, these findings define Zeb1 as a key transcriptional regulator that is essential not only for cardiac development but also for adult cardiomyocyte maintenance. Zeb1 appears to act as a molecular switch between hypertrophic and dilated remodeling pathways, modulating gene expression programs depending on the pathophysiological context. Moreover, the striking sexual dimorphism in the response to Zeb1 loss raises critical questions about hormonal or sex chromosome-related modulators of Zeb1 function in the heart.

Future studies should explore the upstream regulators of Zeb1 translational control during cardiac stress and investigate how ZEB1 interacts with other cardiac transcription factors or RNA-binding proteins such as CPEB4 and RBM20. Ultimately, our study places Zeb1 at an important junction in the transcriptional network governing cardiac structure and function.

Conclusion

In conclusion, our study reveals Zeb1 as a pivotal transcriptional regulator essential for maintaining cardiomyocyte identity, structural integrity, and function. Through an integrative approach combining genetic manipulation and functional assays, we demonstrate that Zeb1 responds dynamically to cardiac stress at the protein level and plays a dual role in the heart, supporting homeostasis under normal conditions while driving pathology when dysregulated. Zeb1OE promotes hypertrophy, fibrosis, and contractile dysfunction, whereas its loss leads to spontaneous heart failure, particularly pronounced in females, along with disrupted sarcomeric organization and mitochondrial architecture. These structural and functional impairments are accompanied by a reactivation of epithelial gene expression, underscoring Zeb1's role in preserving the mesenchymal-like phenotype of mature cardiomyocytes. Our findings highlight a previously underappreciated link between EMT-associated transcriptional networks and cardiac disease, positioning Zeb1 as both a guardian of cardiac homeostasis and a potential contributor to maladaptive remodeling. Therapeutic strategies that modulate Zeb1 activity or its downstream targets in a context-dependent manner may open new avenues for treating heart failure and related cardiovascular conditions.

Clinical Relevance:

Zeb1 expression is post-transcriptionally altered in both hypertrophic and dilated cardiomyopathies. Deletion of Zeb1 in murine hearts is sufficient to induce severe cardiac dysfunction which is associated with sarcomeric disorganization, mitochondrial dysfunction, and progressive cardiac deterioration. The observed sex-specific effects, with females showing greater susceptibility, highlight the need for gender-informed

approaches in cardiovascular research and treatment. Furthermore, the identification of Zeb1-driven transcriptional networks and their role in maladaptive hypertrophic remodeling may uncover novel molecular targets. Targeting Zeb1 or its downstream effectors could offer innovative therapeutic strategies for preventing or reversing heart failure progression.

Limitations of this study:

This study offers critical insights into Zeb1's role in cardiac physiology, especially in sex-specific remodeling and dysfunction. However, its developmental confounding, species/model limitations, incomplete sex hormone analysis, and limited adult cardiomyocyte function assessment restrict the broader application of these findings. Addressing these in the future will be essential for therapeutic targeting or biomarker development related to Zeb1 in cardiac disease.

Acknowledgement:

PG, NF, VK, and MV acknowledge the CRC1550 and the DZHK (German Centre for Cardiovascular Research) Partner Site Heidelberg/Mannheim. VK acknowledges the DFG (German Research Foundation), 552055378. We thank the Electron Microscopy Core Facility (EMCF) at Heidelberg University for assistance with electron microscopic analysis. The EMCF is a DFG-registered research infrastructure (RI 00565). Thanks to Claudia Stroh and Lonny Juergensen for their assistance in data collection and analysis.

References

1. Buckingham M, Meilhac S, Zaffran S. Building the mammalian heart from two sources of myocardial cells. Vol. 6, Nature Reviews Genetics. 2005. p. 826–35.
2. Van Berlo JH, Molkentin JD. An emerging consensus on cardiac regeneration. Vol. 20, Nature Medicine. Nature Publishing Group; 2014. p. 1386–93.
3. insight review articles 198 [Internet]. 2002. Available from: www.nature.com
4. Karbassi E, Fenix A, Marchiano S, Muraoka N, Nakamura K, Yang X, et al. Cardiomyocyte maturation: advances in knowledge and implications for regenerative medicine. Vol. 17, Nature Reviews Cardiology. Nature Research; 2020. p. 341–59.
5. Lamouille S, Xu J, Derynck R. Molecular mechanisms of epithelial-mesenchymal transition. Vol. 15, Nature Reviews Molecular Cell Biology. 2014. p. 178–96.
6. Nieto MA, Huang RYYJ, Jackson RAA, Thiery JPP. EMT: 2016. Vol. 166, Cell. Cell Press; 2016. p. 21–45.
7. Thiery JP, Acloque H, Huang RYJ, Nieto MA. Epithelial-Mesenchymal Transitions in Development and Disease. Vol. 139, Cell. 2009. p. 871–90.
8. Thiery JP, Sleeman JP. Complex networks orchestrate epithelial-mesenchymal transitions. Vol. 7, Nature Reviews Molecular Cell Biology. 2006. p. 131–42.
9. Peinado H, Olmeda D, Cano A. Snail, ZEB and bHLH factors in tumour progression: An alliance against the epithelial phenotype? Vol. 7, Nature Reviews Cancer. 2007. p. 415–28.
10. Brabletz T, Kalluri R, Nieto MA, Weinberg RA. EMT in cancer. Vol. 18, Nature Reviews Cancer. Nature Publishing Group; 2018. p. 128–34.
11. Sánchez-Tilló E, Lázaro A, Torrent R, Cuatrecasas M, Vaquero EC, Castells A, et al. ZEB1 represses E-cadherin and induces an EMT by recruiting the SWI/SNF chromatin-remodeling protein BRG1. Oncogene. 2010 Jun 17;29(24):3490–500.
12. Gheldof A, Berx G. Chapter Fourteen - Cadherins and Epithelial-to-Mesenchymal Transition. In: van Roy F, editor. Progress in Molecular Biology and Translational Science [Internet]. Academic Press; 2013. p. 317–36. Available from: https://www.sciencedirect.com/science/article/pii/B9780123943118000145
13. Siles L, Ninfali C, Cortés M, Darling DS, Postigo A. ZEB1 protects skeletal muscle from damage and is required for its regeneration. Nat Commun. 2019 Dec 1;10(1).
14. Zhang P, Sun Y, Ma L. ZEB1: At the crossroads of epithelial-mesenchymal transition, metastasis and therapy resistance. Vol. 14, Cell Cycle. Landes Bioscience; 2015. p. 481–7.
15. Wellner U, Schubert J, Burk UC, Schmalhofer O, Zhu F, Sonntag A, et al. The EMT-activator ZEB1 promotes tumorigenicity by repressing stemness-inhibiting microRNAs. Nat Cell Biol. 2009 Dec;11(12):1487–95.
16. Krebs AM, Mitschke J, Losada ML, Schmalhofer O, Boerries M, Busch H, et al. The EMT-activator Zeb1 is a key factor for cell plasticity and promotes metastasis in pancreatic cancer. Nat Cell Biol. 2017 May 1;19(5):518–29.
17. Chen T, Pan P, Wei W, Zhang Y, Cui G, Yu Z, et al. Expression of Zeb1 in the differentiation of mouse embryonic stem cell. Open Life Sci. 2022 Jan 1;17(1):455–62.

18. Zhao Q, Shao T, Zhu Y, Zong G, Zhang J, Tang S, et al. An MRTF-A–ZEB1–IRF9 axis contributes to fibroblast–myofibroblast transition and renal fibrosis. Exp Mol Med. 2023 May 1;55(5):987–98.
19. Yao L, Conforti F, Hill C, Bell J, Drawater L, Li J, et al. Paracrine signalling during ZEB1-mediated epithelial–mesenchymal transition augments local myofibroblast differentiation in lung fibrosis. Cell Death Differ. 2019 May 1;26(5):943–57.
20. Liu Y, El-Naggar S, Darling DS, Higashi Y, Dean DC. ZEB1 Links Epithelial-Mesenchymal Transition and Cellular Senescence [Internet]. Available from: http://www.upstate.com/misc/protocol
21. Madany M, Thoma T, Edwards LA. The Curious Case of ZEB1. Discoveries [Internet]. 2018 Dec 31;6(4):e86. Available from: https://www.discoveriesjournals.org/discoveries/D.2018.04.PA-Edwards.DOI
22. Cencioni C, Spallotta F, Savoia M, Kuenne C, Guenther S, Re A, et al. Zeb1-Hdac2-eNOS circuitry identifies early cardiovascular precursors in naive mouse embryonic stem cells. Nat Commun. 2018 Dec 1;9(1).
23. Li H, Zou J, Yu XH, Ou X, Tang CK. Zinc finger E-box binding homeobox 1 and atherosclerosis: New insights and therapeutic potential. Vol. 236, Journal of Cellular Physiology. John Wiley and Sons Inc; 2021. p. 4216–30.
24. Zeisberg EM, Tarnavski O, Zeisberg M, Dorfman AL, McMullen JR, Gustafsson E, et al. Endothelial-to-mesenchymal transition contributes to cardiac fibrosis. Nat Med. 2007 Aug;13(8):952–61.
25. Brabletz S, Lasierra Losada M, Schmalhofer O, Mitschke J, Krebs A, Brabletz T, et al. Generation and characterization of mice for conditional inactivation of Zeb1. Genesis. 2017 Apr 1;55(4).
26. Ackers-Johnson M, Li PY, Holmes AP, O'Brien SM, Pavlovic D, Foo RS. A Simplified, Langendorff-Free Method for Concomitant Isolation of Viable Cardiac Myocytes and Nonmyocytes from the Adult Mouse Heart. Circ Res. 2016 Sep 30;119(8):909–20.
27. Roehr JT, Dieterich C, Reinert K. Flexbar 3.0 - SIMD and multicore parallelization. Bioinformatics. 2017 Sep 15;33(18):2941–2.
28. Langmead B, Salzberg SL. Fast gapped-read alignment with Bowtie 2. Nat Methods. 2012;9(4):357–9.
29. Dobin A, Davis CA, Schlesinger F, Drenkow J, Zaleski C, Jha S, et al. STAR: Ultrafast universal RNA-seq aligner. Bioinformatics. 2013 Jan;29(1):15–21.
30. Liao Y, Smyth GK, Shi W. The R package Rsubread is easier, faster, cheaper and better for alignment and quantification of RNA sequencing reads. Nucleic Acids Res. 2019 May 1;47(8).
31. Ewels P, Magnusson M, Lundin S, Käller M. MultiQC: Summarize analysis results for multiple tools and samples in a single report. Bioinformatics. 2016 Oct 1;32(19):3047–8.
32. Chen Y, Chen L, Lun ATL, Baldoni PL, Smyth GK. edgeR v4: powerful differential analysis of sequencing data with expanded functionality and improved support for small counts and larger datasets. Nucleic Acids Res. 2025 Jan 27;53(2).
33. Gu Z, Eils R, Schlesner M. Complex heatmaps reveal patterns and correlations in multidimensional genomic data. Bioinformatics. 2016 Sep 15;32(18):2847–9.

34. Finke D, Schanze LM, Schreiter F, Kreußer MM, Katus HA, Backs J, et al. Histone deacetylase 4 deletion broadly affects cardiac epigenetic repression and regulates transcriptional susceptibility via H3K9 methylation. J Mol Cell Cardiol. 2022 Jan 1;162:119–29.
35. Ramírez F, Dündar F, Diehl S, Grüning BA, Manke T. DeepTools: A flexible platform for exploring deep-sequencing data. Nucleic Acids Res. 2014 Jul 1;42(W1).
36. Judge DP, Neamatalla H, Norris RA, Levine RA, Butcher JT, Vignier N, et al. Targeted Mybpc3 Knock-Out Mice with Cardiac Hypertrophy Exhibit Structural Mitral Valve Abnormalities. J Cardiovasc Dev Dis [Internet]. 2015;2(2):48–65. Available from: https://www.mdpi.com/2308-3425/2/2/48
37. Koelemen J, Gotthardt M, Steinmetz LM, Meder B. Rbm20-related cardiomyopathy: Current understanding and future options. Vol. 10, Journal of Clinical Medicine. MDPI; 2021.
38. Bak ST, Harvald EB, Ellman DG, Mathiesen SB, Chen T, Fang S, et al. Ploidy-stratified single cardiomyocyte transcriptomics map Zinc Finger E-Box Binding Homeobox 1 to underly cardiomyocyte proliferation before birth. Basic Res Cardiol. 2023 Dec 1;118(1).
39. Liu H, Bersell K, Kühn B. Isolation and characterization of intact cardiomyocytes from frozen and fresh human myocardium and mouse hearts. In: Methods in Molecular Biology. Humana Press Inc.; 2021. p. 199–210.
40. Gladka MM, Kohela A, Molenaar B, Versteeg D, Kooijman L, Monshouwer-Kloots J, et al. Cardiomyocytes stimulate angiogenesis after ischemic injury in a ZEB2-dependent manner. Nat Commun. 2021 Dec 1;12(1).
41. Skrypek N, Bruneel K, Vandewalle C, De Smedt E, Soen B, Loret N, et al. ZEB2 stably represses RAB25 expression through epigenetic regulation by SIRT1 and DNMTs during epithelial-to-mesenchymal transition. Epigenetics Chromatin. 2018 Nov 16;11(1).

Main Figures

Figure 1. Regulation of ZEB1 protein expression in cardiomyopathy models. (a) Immunoblot quantification shows significantly reduced ZEB1 protein levels in ICM (N=8) and DCM (N=8) compared to NF (N=5) hearts. (b) Increased ZEB1 protein expression in Mybpc3 knockout mice, a model of HCM (N=3/group). (c) Reduced ZEB1 protein expression in left ventricular tissue from Rbm20 knockout mice exhibiting DCM (N=3/group). (Dilated cardiomyopathy: DCM, Ischemic cardiomyopathy: ICM, Knockout: KO, Myosin binding protein C3: Mybpc3, Non-failing: NF, Ribosome binding protein 20: Rbm20, Zinc finger E-box binding homeobox 1: Zeb1).

Figure. 2. Zeb1 overexpression promotes cardiomyocyte hypertrophy *in vitro* and *in vivo*. (a,b) Zeb1OE in NRCMs, with/without PE, increases Zeb1 protein/mRNA. (c) Representative immunofluorescence images of NRCMs (sarcomeric α-actinin - green, Zeb1 - red, and DAPI - blue) showing increased cell size in Zeb1OE cells. (d) Quantification of NRCM cell surface area (n = 200/group). (e) qRT-PCR showing *Nppa* expression and downregulation of *Myh6* (n=5/group). (f) Schematic showing AAV9-mediated, cardiomyocyte-specific Zeb1 overexpression in adult mice. (g) Western blot confirming Zeb1 upregulation in the left ventricle tissue lysates of control and Zeb1OE mice (N=4/group). (h) Immunohistochemistry confirming the cardiomyocyte specific upregulation of Zeb1 (sarcomeric α-actinin-green, Zeb1-red, and DAPI-blue). (i) Echocardiography showing representative M-mode image of the left ventricle contractions and graphical representation of significantly reduced ejection fraction, increased LVPW;d (N=6-8/group). (j) Unchanged heart/body weight ratio (N=6/group). (k)

Zeb1 OE hearts show elevated *Nppa/Nppb* expression (N=6-8/group). (Control: Co, Left ventricular posterior wall thickness in diastole: LVPW;d, Phenylephrine: PE, Zeb1 overexpression: Zeb1OE).

Figure. 3. Cardiomyocyte-specific Zeb1 deletion leads to progressive cardiac dysfunction and remodeling. (a) Zeb1cKO mice were generated using Cre-loxP and validated via western blot and showing Zeb1 loss in the heart but not liver. (b) Immunostaining of left ventricle tissue, showing Zeb1 loss only in cardiomyocyte nuclei (sarcomeric α-actinin-green, Zeb1-red, and DAPI-blue). (c) Echocardiography showing representative M-mode image of the left ventricle contractions of 25 week and older male mice. (d) Echocardiographic analysis showing significantly reduced EF and increased LV volume/diameter in 12-week-old Zeb1cKO mice, with further EF decline by 25 weeks (N=5-9/group). (e) Gross morphology and histology showing ventricular dilation of 25 week and older male mice hearts fixed in formaldehyde. (f) Unchanged heart/body weight ratio (N=5-22/group). (g) qRT-PCR showing significantly elevated *Nppa/Nppb* in 25 weeks and older Zeb1cKO male left ventricle lysates (N=6/group). (Cardiomyocytes: CM, Cardiomyocyte-specific Zeb1 conditional knockout: Zeb1cKO, Ejection fraction: EF, Left ventricle: LV, Wild type: WT).

Figure. 4. Female Zeb1 knockout mice exhibit severe cardiac dysfunction. (a) Percent of survival calculated by counting the number of mice dying naturally in the animal facility showing reduced survival of female Zeb1cKO mice post-20 weeks. (b) M-mode image showing severe LV dilation of 25 weeks and older female Zeb1cKOs. (c) Age wise

comparison of EF, LV volume, and diameter, highly significant reduction of EF at old age compared to young WT. The 25 weeks and older mice show increased left ventricle volume and diameter (N=4-12/group). (d) Significant increase in Heart/body weight ratio by ≥25 weeks (N=4-12/group). (e) Masson's Trichrome staining and heart images after formaldehyde fixation confirms dilation without fibrosis in 25 weeks and older female Zeb1cKO mice. (f) *Nppa/Nppb* levels are elevated in Zeb1cKO left ventricle lysates. (g) Schematic representation of Zeb1icKO model and confirmation of cardiomyocyte specific Zeb1 loss by western blot of adult cardiomyocytes. (h) M-mode image showing slight LV dilation of female Zeb1cKOs 7 weeks post tamoxifen injection. (i) EF, LV volume, and diameter measurements taken from the echocardiography showing only EF reduction in Zeb1icKO mice without any change in LV volume and diameter (N=10/group). (j) Unchanged heart/body weight ratio (N=4-6/group). (Cardiomyocyte-specific Zeb1 conditional knockout: Zeb1cKO, Cardiomyocyte-specific Zeb1 inducible conditional knockout: Zeb1icKO, Ejection fraction: EF, Left ventricle: LV, Wild type: WT).

Figure. 5. Zeb1 deletion disrupts sarcomeric structure, contributing to cardiomyocyte remodeling. (a) TEM of 25-week-old female Zeb1cKO hearts revealed severe sarcomeric disarray and mitochondrial abnormalities (N=2/group). (b) Sarcomere length quantified from the TEM images. (c, d) Sarcomere length quantified from isolated ACMs from 8-week-old male Zeb1cKO mice, measured via IonOptix. (e, f, g) MLP2 immunostaining of female Zeb1cKO heart sections revealed increased sarcomere length and Z-disc thickness. (h, I, j) Similar alterations were observed in female Zeb1icKO hearts. (Adult cardiomyocytes: ACMs, Cardiomyocytes: CM, Cardiomyocyte-specific

Zeb1 conditional knockout: Zeb1cKO, Cardiomyocyte-specific Zeb1 inducible conditional knockout: Zeb1icKO, Muscle LIM-protein 2: MLP2, Transmission electron microscopy: TEM, Wild type: WT).

Figure. 6. Bulk RNA-seq, motif analysis identifies Zeb1 repressing epithelial genes. (a) Bulk RNA-Seq of left ventricle tissue from ≥25-week-old female Zeb1cKO vs. WT mice. (b) Dot-plot of top 20 GO enrichment terms for biological process of upregulated differentially expressed genes (DEGs) identified from the RNA-seq of Zeb1cKO vs WT female. Highlighted are the genes involved in ECM organization and epithelial programs. (c) De novo motif analysis (HOMER) identified Zeb1 as the top-enriched motif. (d) Volcano plot showing up and down regulated DEGs and ZEB1 binding motif genes overlapped. (e) Percent enrichment showing Zeb1 motif genes enriched in 3.67% of upregulated vs. 1.34% of downregulated DEGs. (f, g) Epithelial markers *Cdh1* and *Krt8* were significantly upregulated at mRNA and protein levels in Zeb1cKO LVs (N=4/group). (Cardiomyocyte-specific Zeb1 conditional knockout: Zeb1cKO, Gene ontology: GO, Left ventricle: LV, log fold change: logFC, Wild type: WT).

Figure 7. Zeb1 ChIP-seq and Transcriptomics Integration Reveals Direct Regulatory Programs in Cardiomyocytes. (a) Schematic of experimental strategy using neonatal cardiomyocytes for ChIP-seq. (b) Peak annotation showing Zeb1 enrichment in intronic (55.2%), exonic (17.8%), intergenic (11.3%), and promoter/TSS regions (12%), with promoter peaks being largest. (c, d) Heatmaps and average plot profiles of all annotated genes and genes with only promoter peaks demonstrating Zeb1 enrichment at TSSs, with

sharper peaks in promoter-bound genes. (e) Gene ontology analysis for biological process of promoter-bound targets identifying enrichment in metabolic and stress-response pathways. (f) Averaged Integrated Gene view of 3 replicates of the Zeb1 ChIP-seq shows Zeb1 peaks at promoters/TSSs of Cdh1 (TSS at the left end of the gene) and Krt8 (TSS at the right end of the gene). (g) Venn diagram of promoter-peak genes (6544), RNA-seq DEGs (2103), and Zeb1 motif genes identified from RNA-seq (246) defines 567 high-confidence novel Zeb1 targets that are common between promoter-peak genes (6544) and Zeb1 motif genes identified from RNA-seq (246). (h) Aggregated signal of promoter-bound genes (n = 24,696), Zeb1 motif genes from RNA-seq (246), and new Zeb1 target genes identified from ChIP-seq (n = 567) shows sharp pre-TSS peaks in both the later groups. (i) Volcano plot of 597 genes common between DEGs from RNA-seq of female Zeb1cKO vs WT and annotated promoter peak containing ChIP-seq genes: 171 downregulated, 396 upregulated. (j) GO terms of the downregulated genes described in the (i) section highlight cytoplasmic, mitochondrial, and t-tubule components, including Acaa2, Atp1a2. (k) Averaged Integrated Gene view of 3 replicates of the Zeb1 ChIP-seq shows a sharp Zeb1 binding peak at the transcription start site of Acaa2 (TSS at the left end of the gene). RNA-seq reveals significant downregulation of *Acaa2* in Zeb1 cKO mice. (l) Averaged Integrated Gene view of 3 replicates of the Zeb1 ChIP-seq shows of Smim20 (TSS at the right end of the gene) display multiple Zeb1 binding peaks across exons and at the transcription start site. *Smim20* expression is significantly reduced in Zeb1cKO mice. (Cardiomyocyte-specific Zeb1 conditional knockout: Zeb1cKO, Chromatin immunoprecipitation sequencing: ChIP-seq, differentially expressed genes:

DEGs, Left ventricle: LV, log fold change: logFC, Transcription end site: TES, Transcription start site: TSS, Wild type: WT).

Figure 8. Zeb1 regulates mitochondrial integrity, abundance, and bioenergetic function. (a) TEM images of cardiac tissue from WT and Zeb1cKO hearts displaying abnormal mitochondrial morphology characterized by disrupted ultrastructure and reduced mitochondrial number in 25 weeks and older Zeb1cKO compared to WT (Arrows indicate damaged mitochondria). (b) Quantification of mitochondrial abundance by qRT–PCR analysis of mtDNA relative to nuclear gDNA in WT and Zeb1cKO heart, liver, and skeletal muscle tissue lysates. (c) Seahorse extracellular flux analysis of OCR in NRVMs transfected with control or Zeb1-targeting siRNA. (d) Basal OCR in Zeb1-depleted cells compared to controls. (e) Maximal respiratory capacity of Zeb1 knockdown cells relative to control upon FCCP-induced uncoupling. (Cardiomyocyte-specific Zeb1 conditional knockout: Zeb1cKO, Carbonyl cyanide-4-(trifluoromethoxy)phenylhydrazone: FCCP, Genomic DNA: gDNA, mitochondrial DNA: mtDNA, Oxygen consumption rate: OCR, Transmission electron microscopy: TEM, Wild type: WT).

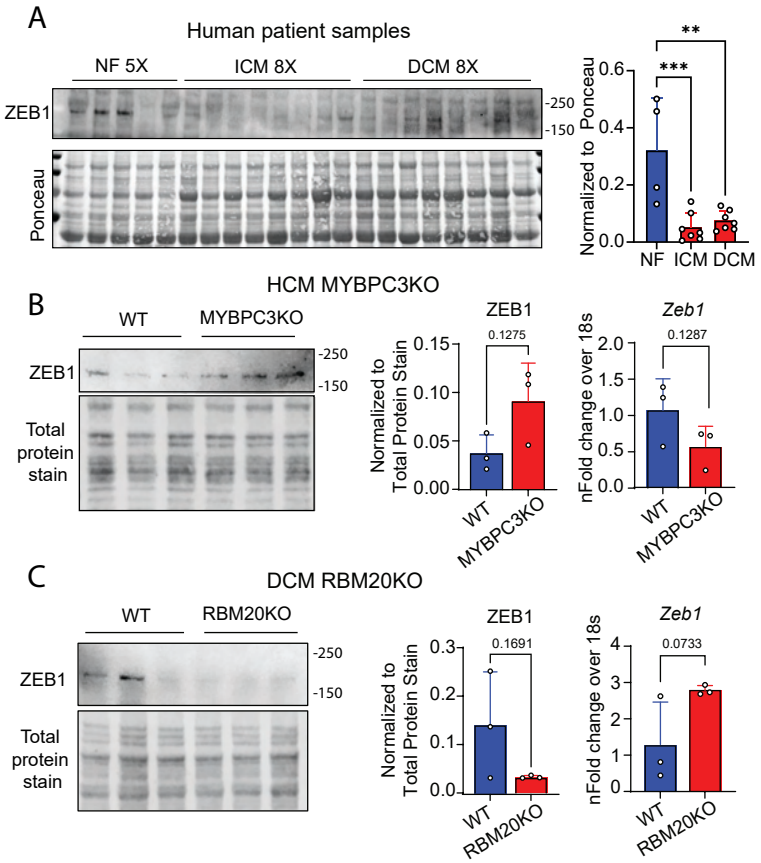

Figure 1. Regulation of ZEB1 protein expression in cardiomyopathy models.

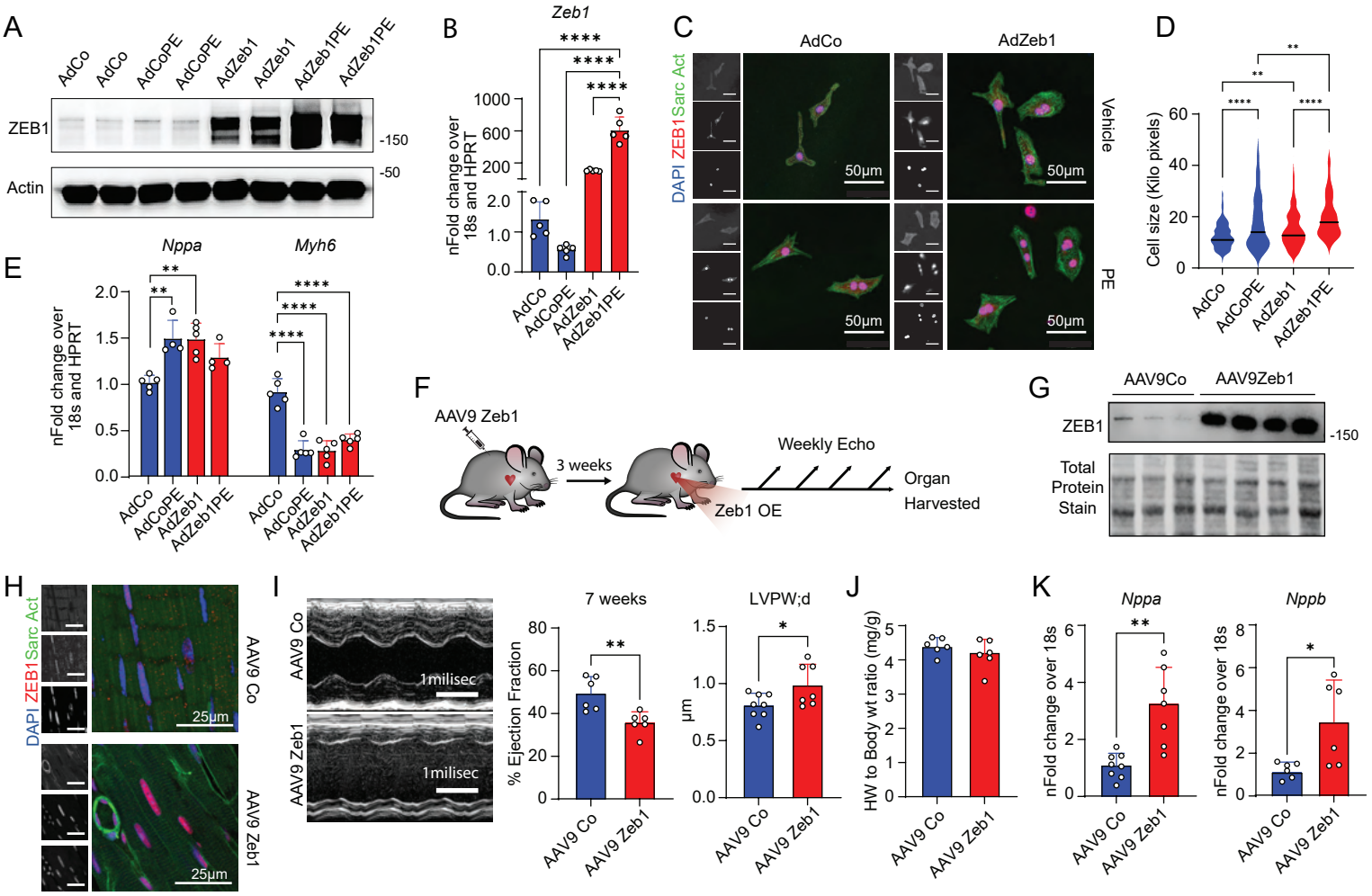

Figure 2. Zeb1 overexpression promotes cardiomyocyte hypertrophy and dysfunction in vitro and in vivo.

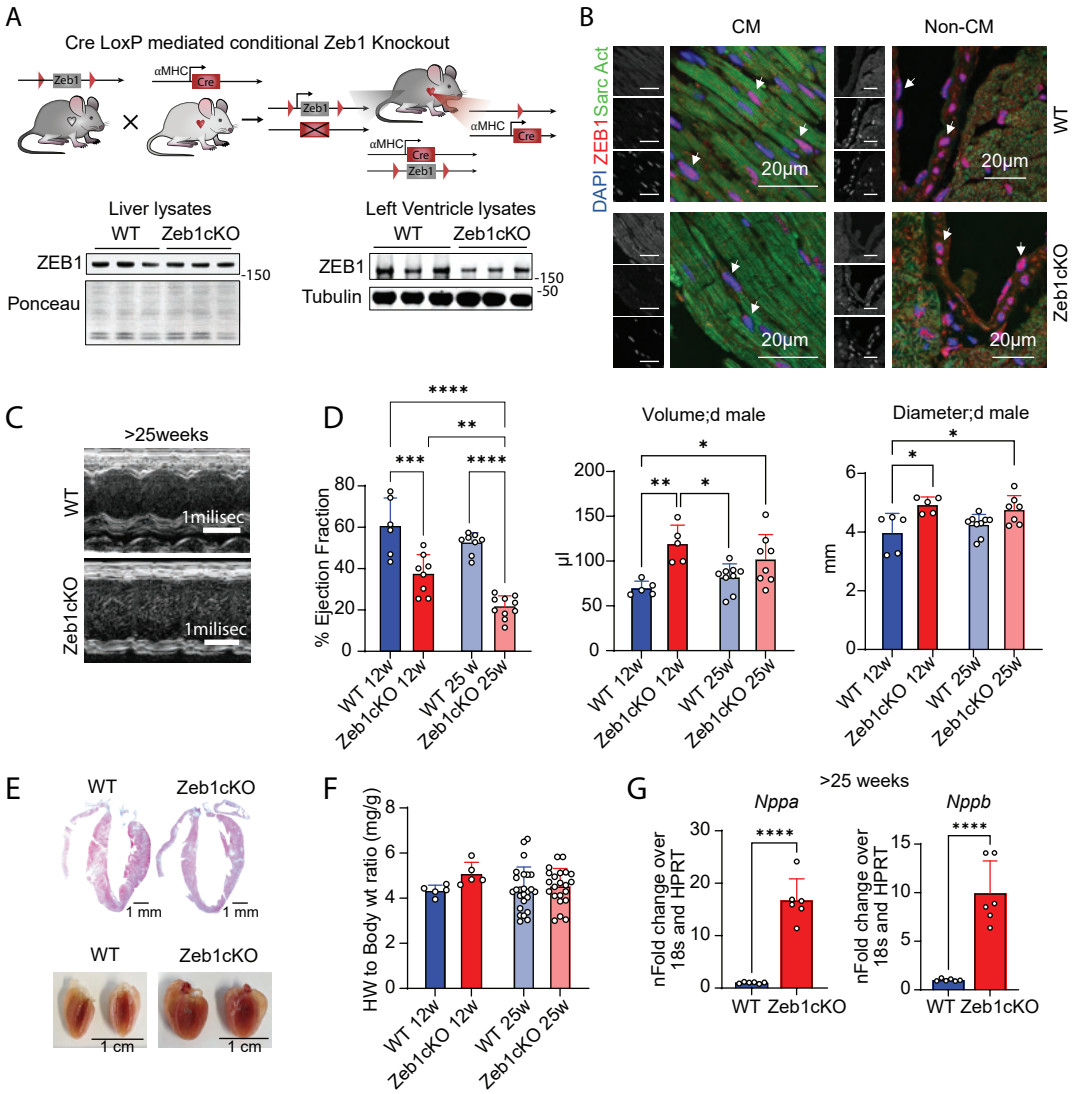

Figure 3. Cardiomyocyte-specific Zeb1 deletion leads to progressive cardiac dysfunction and remodeling.

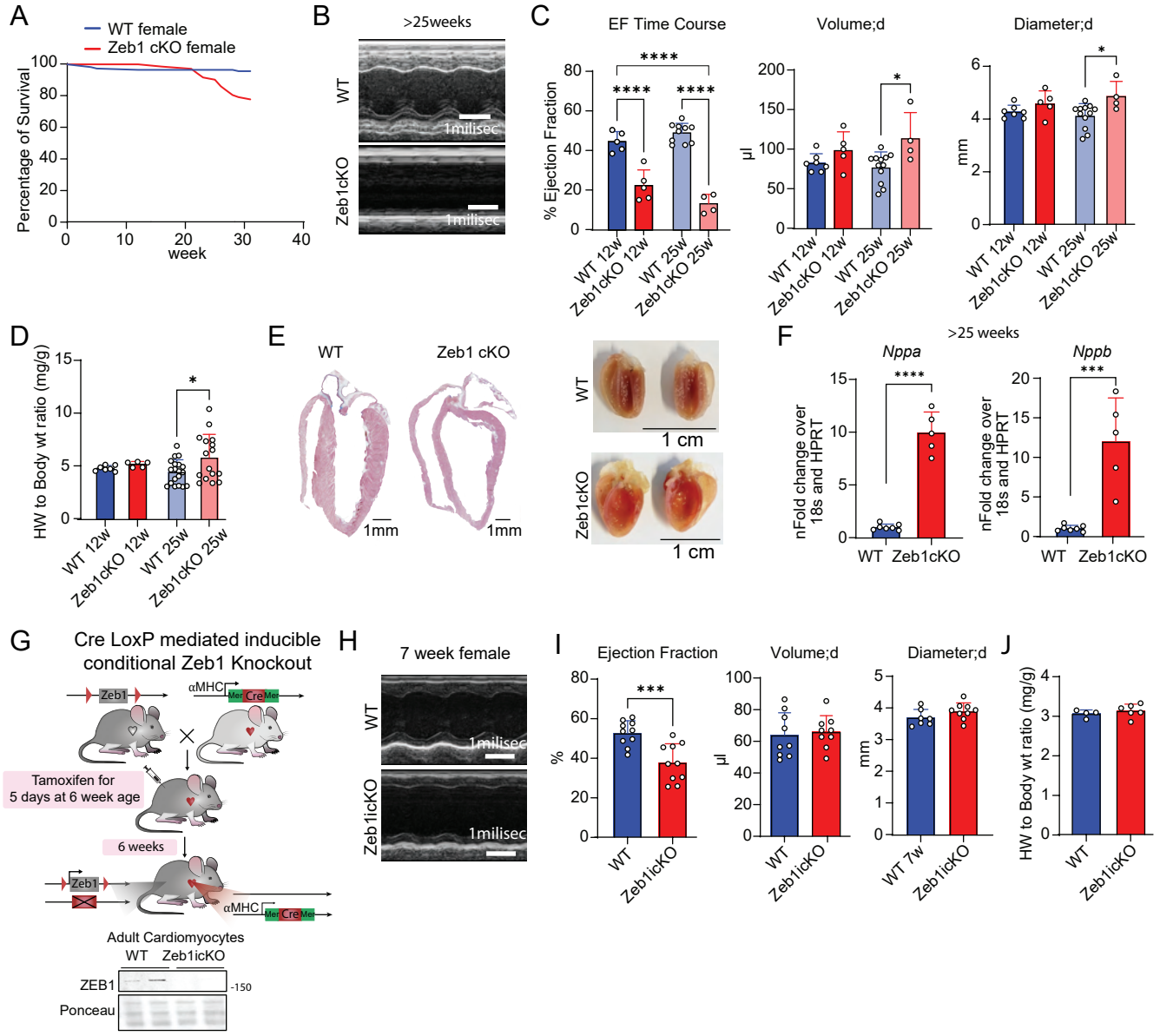

Figure 4. Female Zeb1 cKO mice exhibit severe cardiac dysfunction and reduced survival; inducible KO confirms sex-specific dependency.

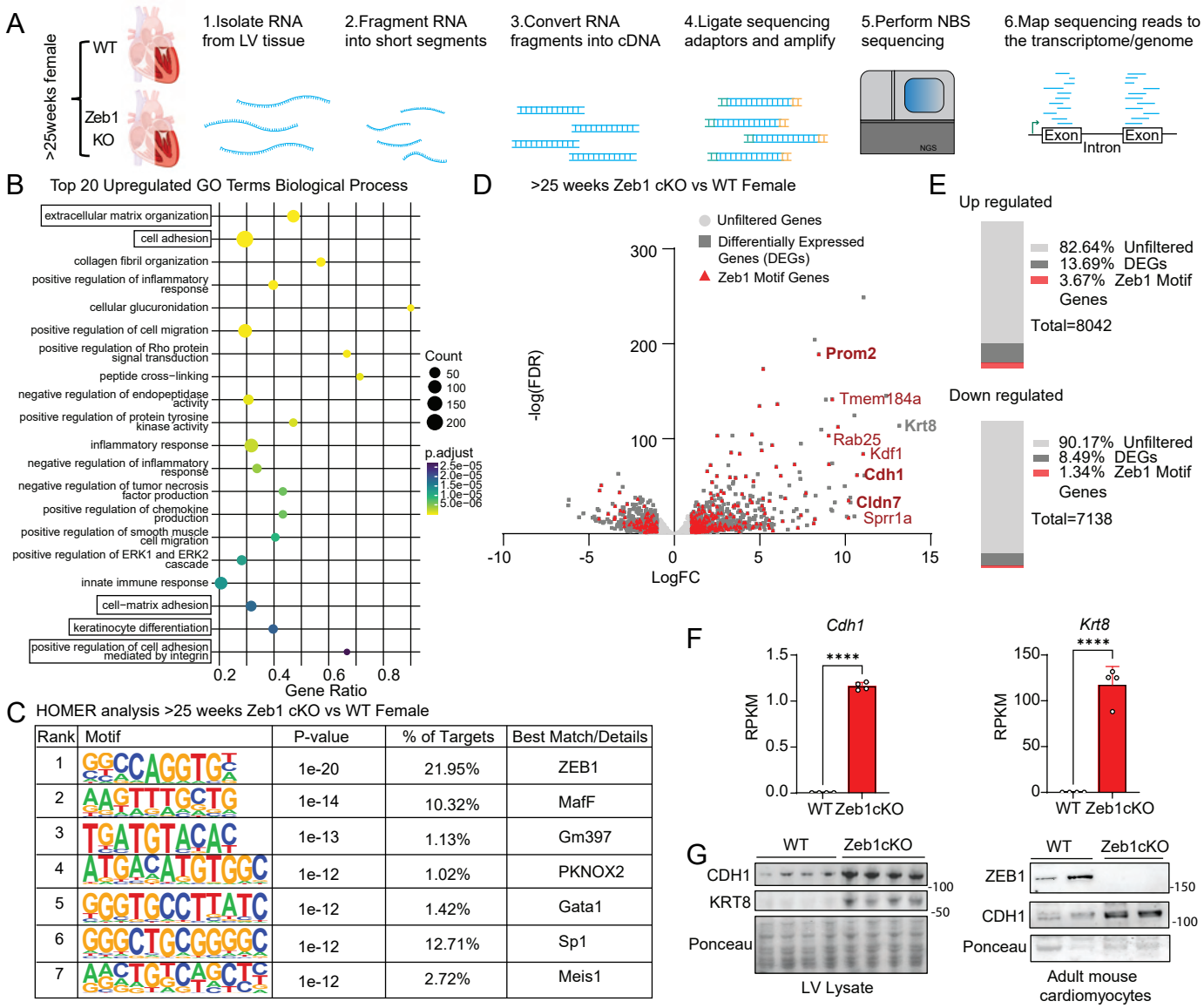

C HOMER analysis >25 weeks Zeb1 cKO vs WT Female

Rank	Motif	P-value	% of Targets	Best Match/Details
1	GGCCAGGTGT	1e-20	21.95%	ZEB1
2	AAGTTTGCTG	1e-14	10.32%	MafF
3	TGATGTACAC	1e-13	1.13%	Gm397
4	ATGACATGTGGC	1e-12	1.02%	PKNOX2
5	GGGTGCCTTATC	1e-12	1.42%	Gata1
6	GGGCTGCGGGGC	1e-12	12.71%	Sp1
7	AACTGTCAGCTC	1e-12	2.72%	Meis1

Figure 6. Bulk RNA-Seq and motif analysis reveal Zeb1 as a key transcriptional repressor of epithelial gene programs in female cardiomyocytes.

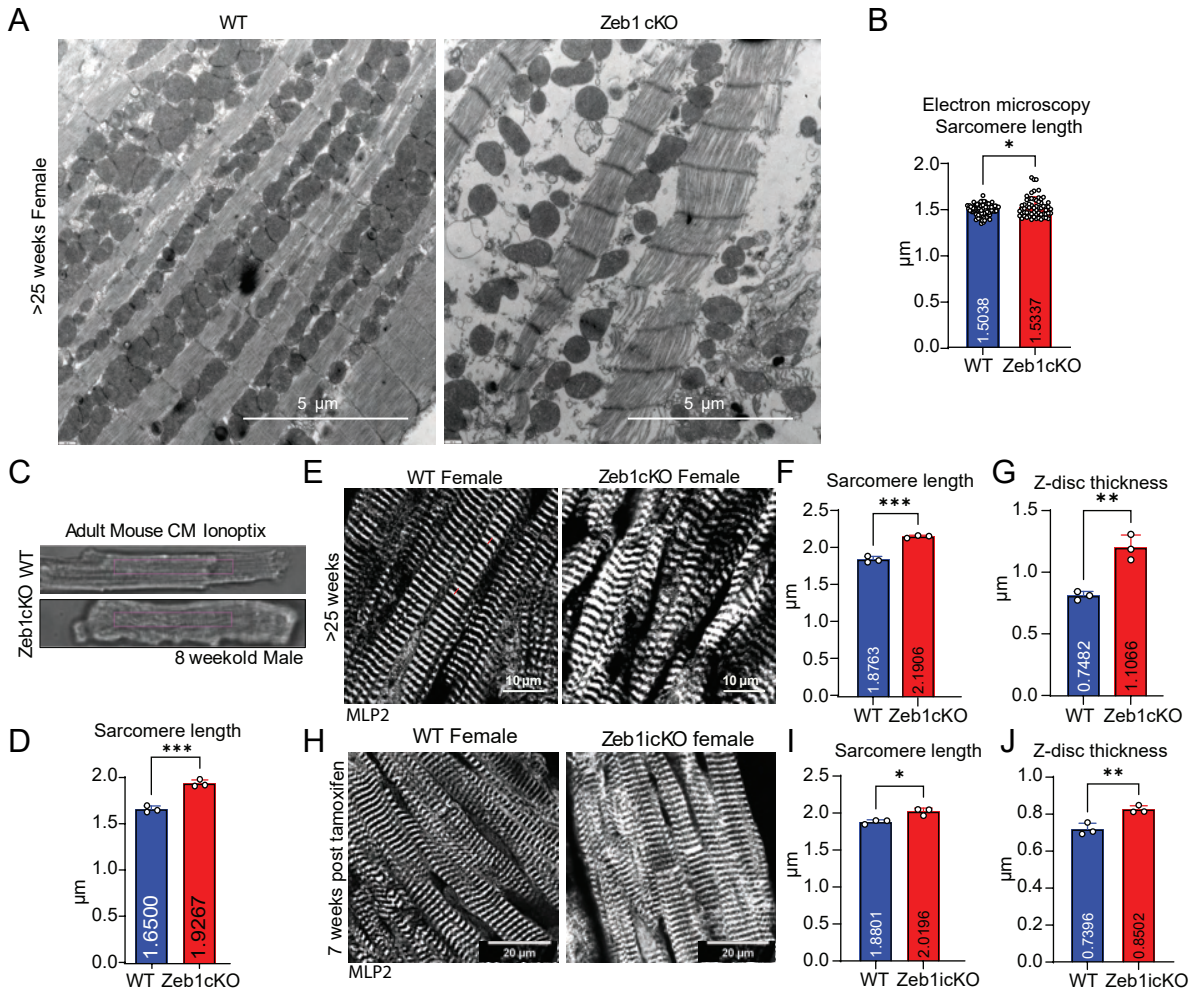

Figure 5. Zeb1 deletion disrupts sarcomeric structure and mitochondrial integrity, contributing to cardiomyocyte remodeling and dysfunction.

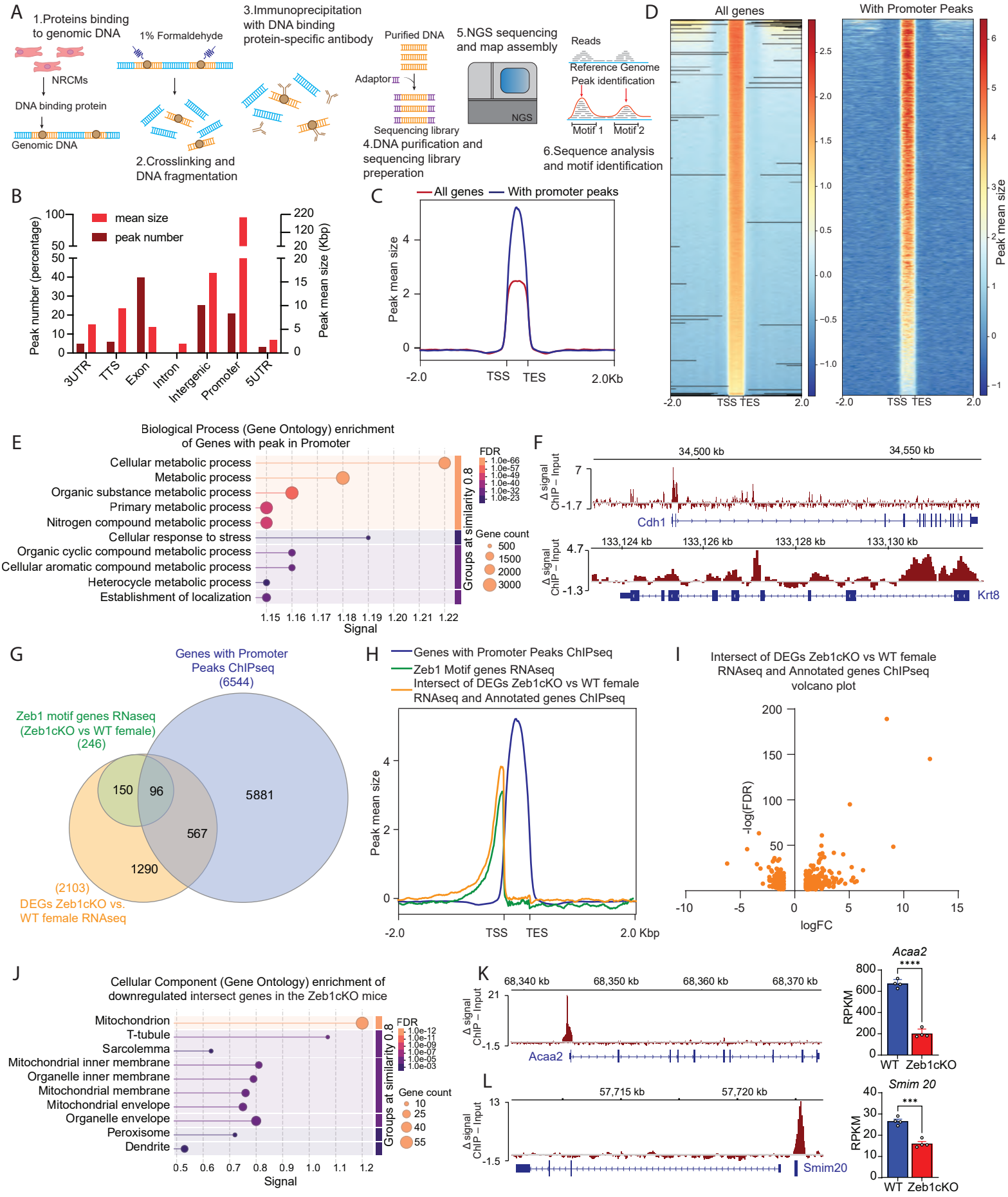

Figure 7. Integration of Zeb1 ChIP-seq and Transcriptomics Reveals Direct Regulatory Programs in Cardiomyocytes.

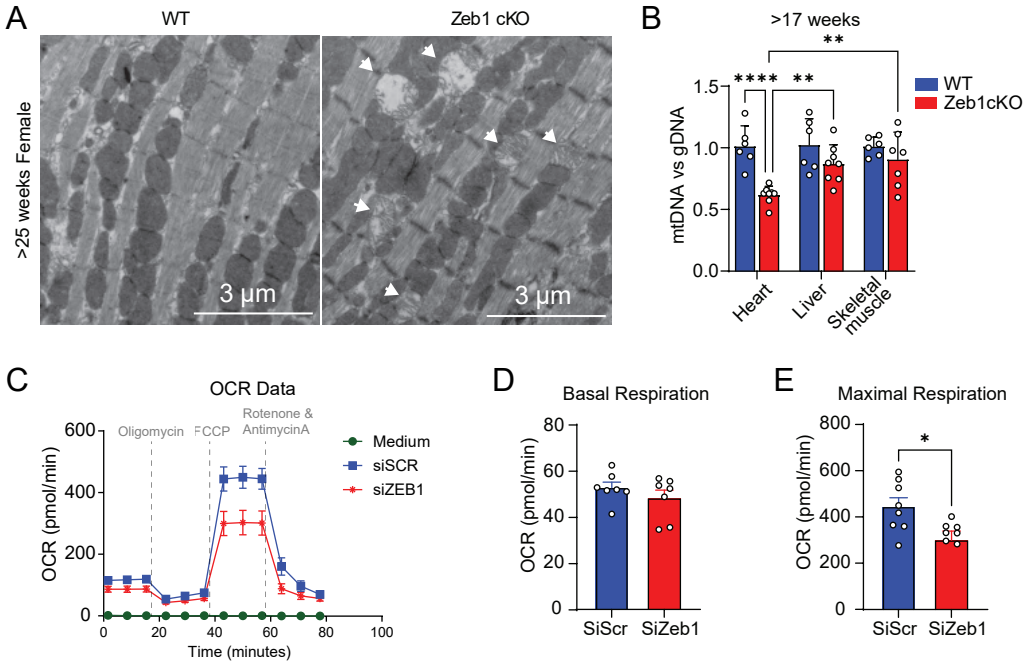

Figure 8. Zeb1 regulates mitochondrial integrity, abundance, and bioenergetic function.

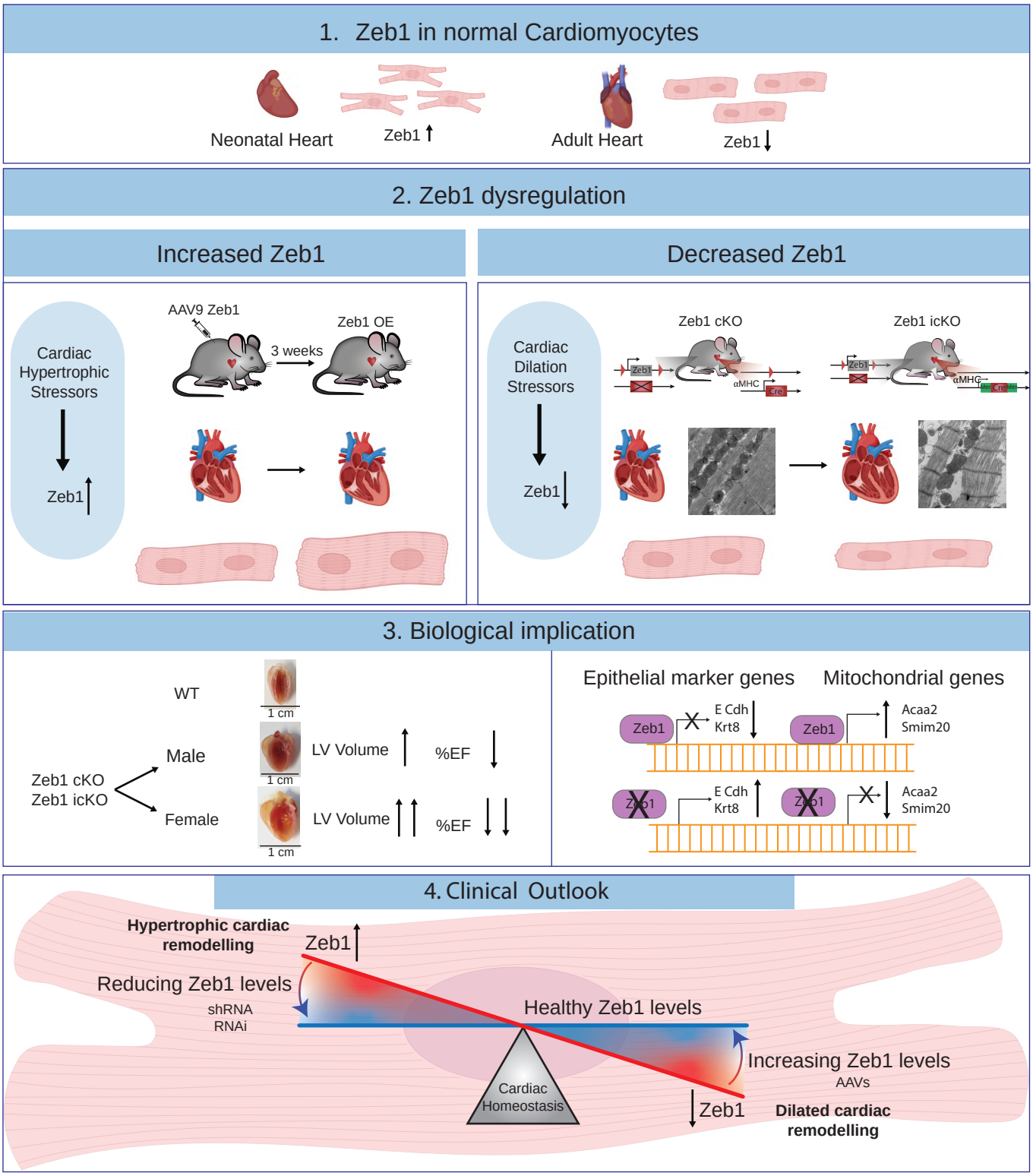

Graphical Abstract / Summary Figure

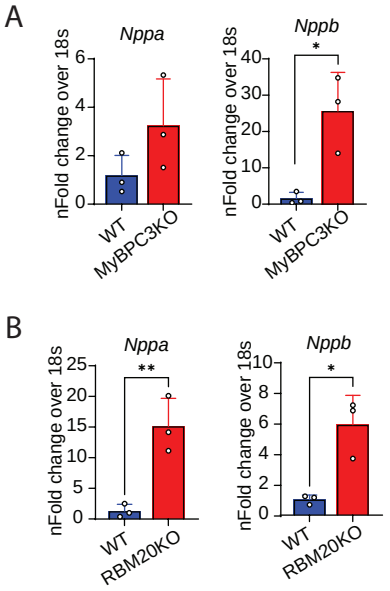

Supplementary Figure. 1

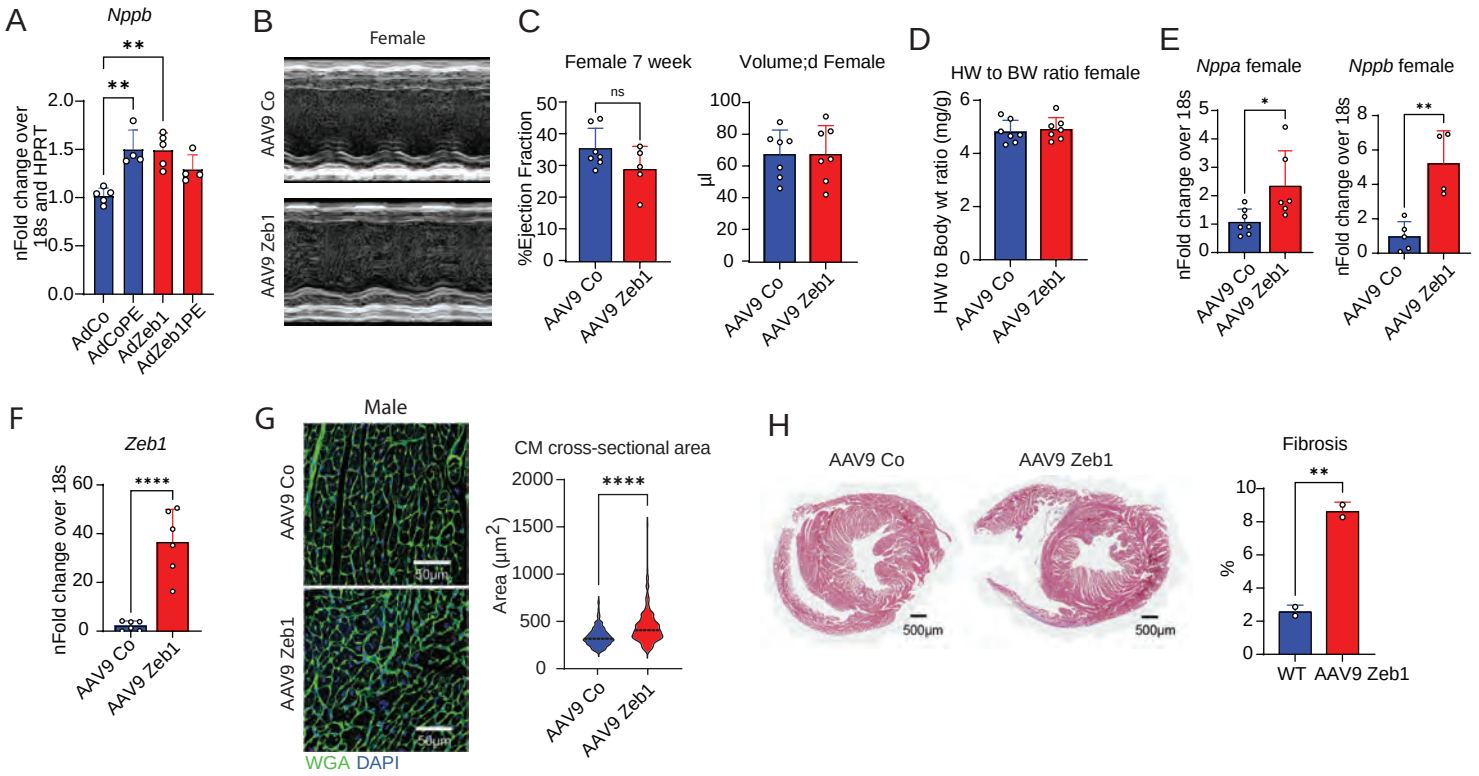

Supplementary Figure. 2

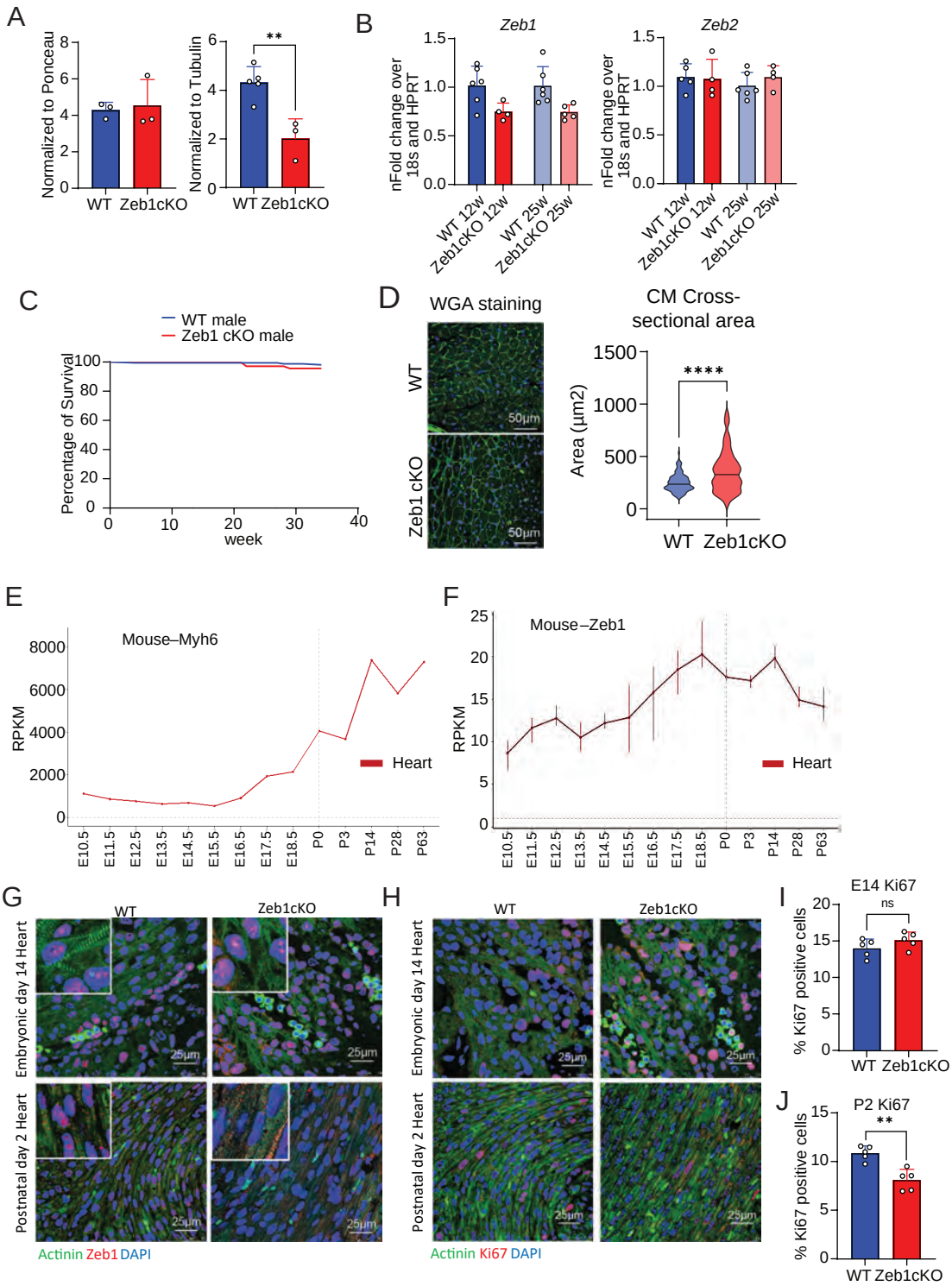

Supplementary Figure. 3

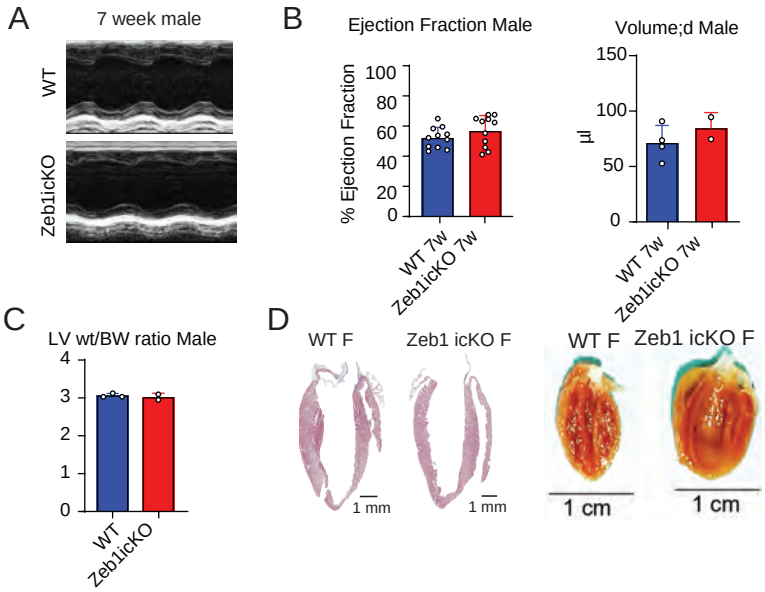

Supplementary Figure. 4

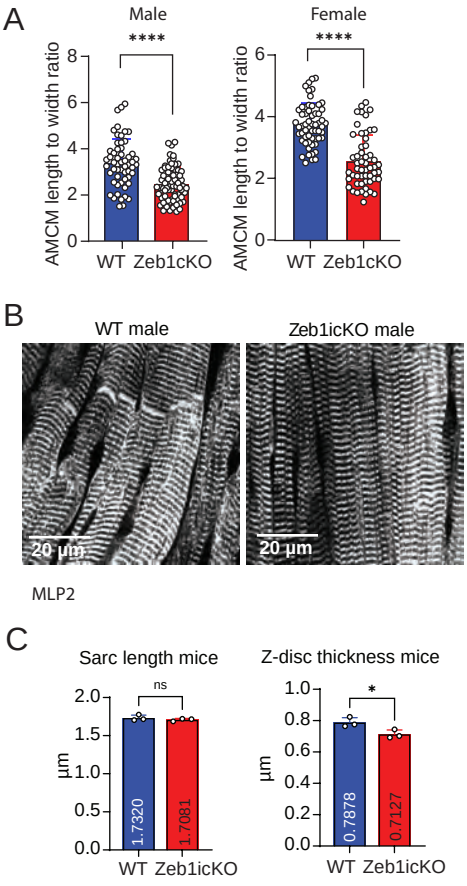

Supplementary Figure. 5

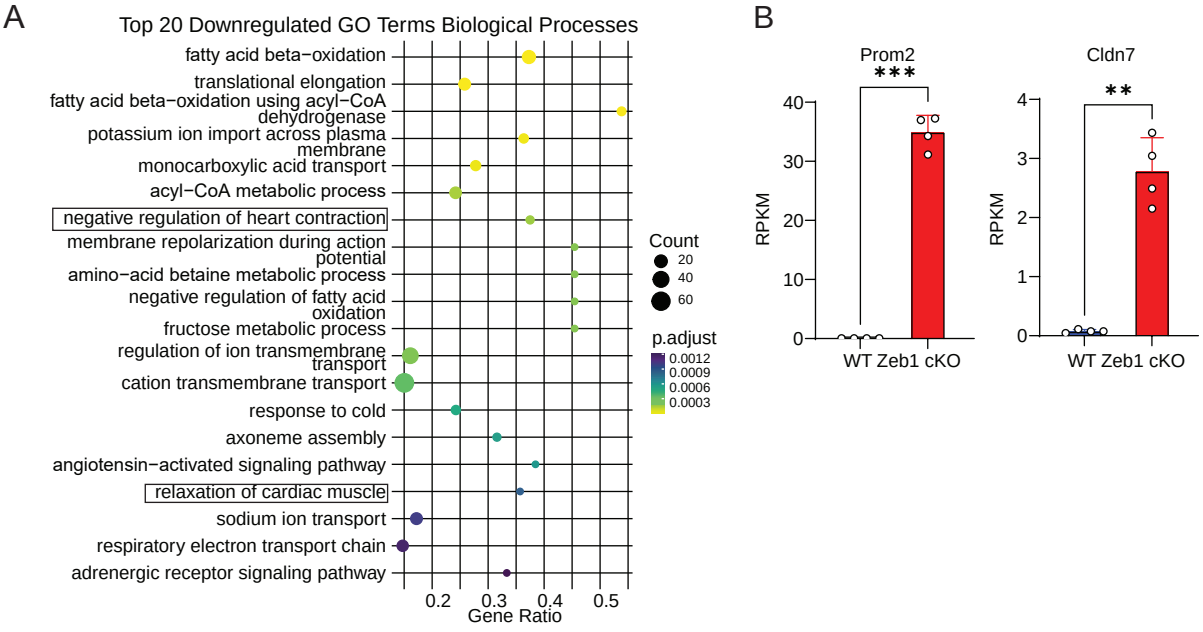

Supplementary Figure. 6

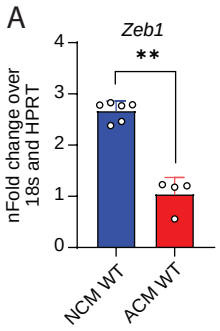

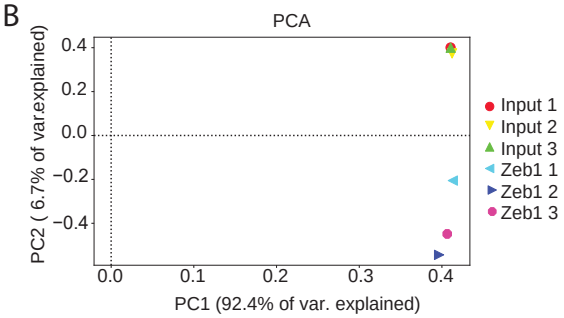

C

Reads		% Aligned reads		Peaks	Annotated peaks
Input	Zeb1 ChIP	Input	Zeb1 ChIP	146,333	71,907
1.51E+08	8.30E+07	93.06	94.40		

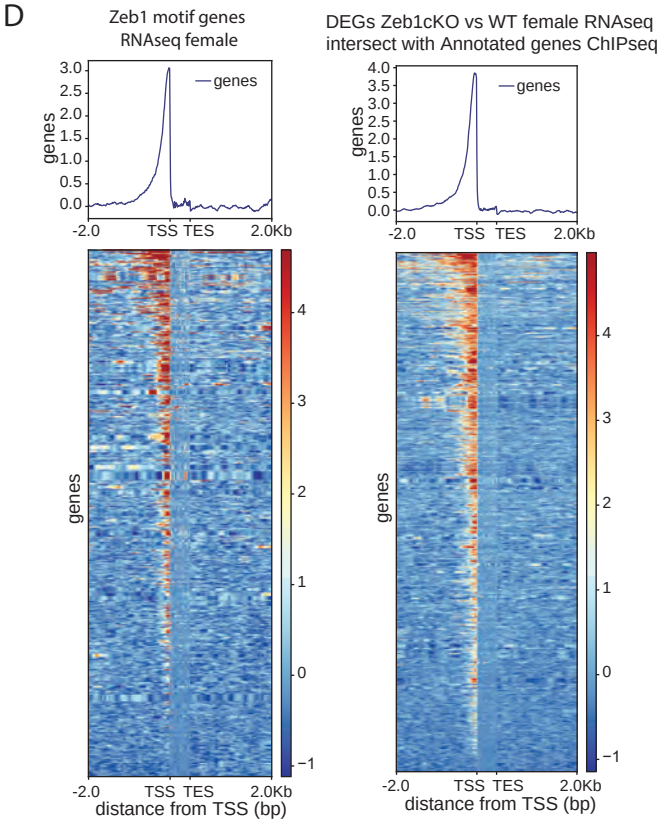

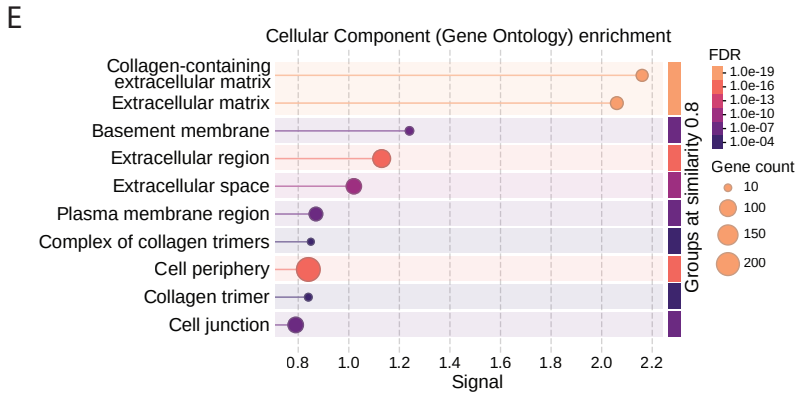

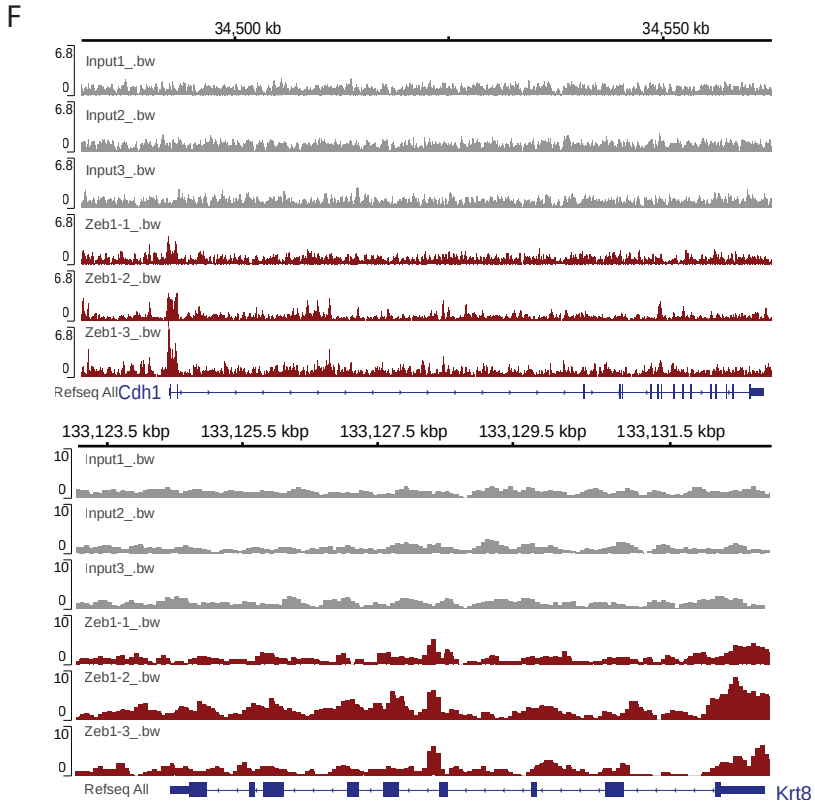

Supplementary Figure. 7

Supplementary Figures

Supplementary Figure 1.

(a, b) *Nppa/Nppb* levels are elevated in Zeb1cKO left ventricle lysates from Mybpc3KO and Rbm20KO mice confirming cardiac dysfunction.

Supplementary Figure 2.

(a) Significantly elevated mRNA levels of *Nppb* in Zeb1OE NRCMs as compared to control virus treated cells like PE treated cells, confirming the cellular hypertrophy due to Zeb1OE. (b) M-mode image showing no significant difference between control and Zeb1OE female mice. (c) EF and LV volume measurement showing no significant change upon Zeb1OE in females (N=5-7/group). (d) Unchanged heart/body weight ratio (N=7/group). (e) Significantly elevated mRNA levels of *Nppb* in Zeb1OE NRCMs as compared to control virus indicating towards pathological remodeling of heart (N=4-7/group). (f) qRT-PCR showing significant overexpression of Zeb1 (N=6/group). (g) WGA staining of formaldehyde fixed paraffin embedded LV tissue sections showing increased cardiomyocyte cross-sectional area. The cross-sectional area is quantified and plotted (n=200 cells/group). (h) Masson's Trichrome staining of cross sections of heart after formaldehyde fixation. %Fibrosis was quantified and a significant increase was seen in the Zeb1 OE hearts (N=2/group).

Supplementary Figure 3.

(a) Western blot quantification normalized to the respective loading controls showing a significant decrease in the ZEB1 levels in LV tissue samples as compared to liver tissue

samples (N=3-5/group). (b) qRT-PCR of Zeb1 and Zeb2 mRNA from the LV tissue lysates from 12 week and 25-week-old Zeb1cKO and WT mice showing reduced levels of Zeb1 mRNA but no change in Zeb2 mRNA levels (N=4-7/group). (c) Percent of survival calculated by counting the number of mice dying naturally in the animal facility showing a normal survival curve of male Zeb1 cKO mice. (d) WGA staining of formaldehyde fixed paraffin embedded LV tissue sections showing increased cardiomyocyte cross-sectional area. The cross-sectional area is quantified and plotted (n=200-250 cells/group). (e, f) Gene expression profile of Myh6 and Zeb1 in mouse generated from "Evo-devo mammalian organs" app from the Kaessmann lab. (g) Immunofluorescence staining for ZEB1 in heart sections from control and Zeb1 conditional knockout (cKO) mice at embryonic day 14 (E14) and postnatal day 2 (P2), confirming efficient Zeb1 deletion by P2 but not at E14. Nuclei were counterstained with DAPI. (h) Representative immunofluorescence images showing Ki67 (a proliferation marker) staining in ventricular sections from E14 and P2 Zeb1 cKO hearts. (i, j) Quantification of Ki67-positive cardiomyocytes reveal a significant decrease in the proportion of proliferating CMs at P2 in Zeb1 cKO hearts compared to E14 (N = 5/group).

Supplementary Figure 4.

(a) M-mode image showing no significant difference between control and Zeb1icKO 7 weeks after tamoxifen injection in male mice. (b) EF and LV volume measurement showing no significant change upon Zeb1icKO 7 weeks after tamoxifen injection in male mice (N=2-11/group). (c) Unchanged left ventricle/body weight ratio in male Zeb1icKO (N=2-3/group). (d) Masson's Trichrome staining and heart images after formaldehyde

fixation shows slight to almost no dilation without fibrosis in 7 weeks post tamoxifen female Zeb1icKO mice.

Supplementary Figure 5.

(a) Cardiomyocytes isolated from formaldehyde-fixed hearts of mice ≥25 weeks showed reduced yield in Zeb1 cKO compared to WT. Zeb1-deficient cells displayed a significantly lower length-to-width ratio, indicating altered morphology in both male and female. (b) CSRP3-based analysis of LV sections from male Zeb1 inducible conditional knockout (icKO) mice. (c) No significant change in sarcomere length and Z-disc thickness (N = 3/group).

Supplementary Figure 6.

(a) Top20 downregulated Gene Ontology (GO) term enrichment analysis for biological processes of female Zeb1cKO vs WT DEGs. (b) RPKM plots of identified epithelial markers Cldn7 (Claudin 7) and Prom2 (Prominin 2) among upregulated DEGs in female Zeb1 KO mice.

Supplementary Figure 7.

(a) qRT-PCR of Zeb1 in isolated cardiomyocytes from postnatal day 2 hearts (NCM) and 8-week-old mouse hearts (ACM). (b) Principal component analysis (PCA) of ChIP-seq datasets. PC1 on the x-axis explaining 92.4% variance and PC2 on the y-axis explaining 6.7% variance. Separated groups of input and Zeb1 samples shows good quality of ChIP-seq (N=3/group). (c) Table showing the alignment statistics of sequencing reads from

input and Zeb1 immunoprecipitated (IP) chromatin. (d) Heatmaps and average plot profiles of Zeb1 motif genes identified from RNA-seq and new Zeb1 motif genes identified by ChIP-seq that overlap with RNA-seq DEGs showing enrichment before TSS, with sharper peaks in promoter regions. (e) Individual IGV tracks of all input and Zeb1 ChIP-seq replicates for Cdh1 and Krt8 showing clear peaks at the TSS and promoter regions on the Zeb1 replicates and nothing in the input replicates.

Statistics and WB loading controls

Data are shown as mean ± SEM. Statistical analysis was performed using unpaired Student's *t*-test or one-way ANOVA (*=$p<0.05$, **=$p<0.01$, ***=$p<0.001$, ****=$p<0.0001$). Tubulin, Actin, Ponceau, and Total protein stain are shown as loading controls. Data are representative of at least three biological replicates.